# Real-time dynamics of IκBα degradation studied with Kusabira-Orange 2 fusion proteins

2016

Nilufar Rahimova

# Table of Contents

## List of Illustrations

# Preface

The nuclear factor-κB (NF-κB) consists of a family of transcription factors, which regulates diverse biological processes, including cell division, apoptosis and many aspects of immunological functions. In resting cells, NF-κB is stabilized by association with its inhibitors of IκB family, being IκBα the major inhibitor protein. NF-κB activation is initiated by a variety of stimuli such as pathogen associated molecules, cytokines and growth factors, which lead to activation of IκB kinase complex (IKK). IKK in turn phosphorylates IκBα, resulting in its degradation via the ubiquitin-mediated proteolytic pathway.

Pathological dysregulation of NF-κB is linked to inflammatory and autoimmune diseases as well as cancers. In these conditions IκBα is being continuously degraded. Although much has been learned about the biochemistry of IκBα degradation, it is unclear what factors control the kinetics and endurance of this process. In order to address this, it is of practical importance to develop sensitive tools to monitor the signal-induced degradation of IκBα in real-time in living cells.

Here, I proposed to develop fusion proteins of IκBα and fluorescent protein monomeric Kusabira-Orange 2 (mKO2) to visualize the dynamic behavior of IκBα degradation in real-time. The technique that has been described should provide a range of possible applications, for example the analysis of the dynamics and biochemical characteristics of IκBα degradation as well as for drug screening of potential proteasomal inhibitors. Moreover, it could be very valuable for analysis of protein-protein interactions in solution using mKO2 fusion proteins.

In this thesis, therefore, I constructed genetically encoded fusion proteins of full-length or fragments of human IκBα and mKO2 linked to its N terminus. Then, I have applied fluorescence based imaging to investigate the kinetics of the IκBα degradation in living cells. I checked the potential of this tool in the evaluation of inhibitors targeting ubiquitin-proteasomal pathway. Finally, I used computational approach to generate models and constructed detailed molecular dynamics simulations of fusion proteins in explicit solvent to investigate the structure-activity relationship of the degradation process.

This dissertation consists of three parts. First, construction of recombinant vectors and *in vitro* evaluation of fusion proteins are shown in Chapter I. In Chapter II, kinetics of IκBα degradation is investigated *in vitro* using HeLa cells. In Chapter III, structural properties of fusion proteins are analyzed using computational methods.

Studies in this dissertation demonstrate the development of fluorescent IκBα fusion proteins and their application to investigate the degradation and kinetics of IκBα in living cells as well as potential of this platform to be used as first-pass screening tool for inhibitors targeting NF-κB pathway. This work is to the best of our knowledge original, except where acknowledgements and references were made to previous works. Neither this, nor any other considerably similar work has been or is being considered to any other degree or diploma at any other institution.

## Background and Strategy

The NF-κB transcription factor controls a range amount of target genes that play important role in cell survival, inflammation and immune system [1-3]. Initially NF-κB was described as a DNA-binding protein with affinity to the kappa immunoglobulin-light chain enhancer in B cells [4]. Later studies revealed that NF-κB activity is induced in almost all mammalian cell types and is involved in cellular responses to wide variety of stimuli, with important roles in cell division, regulation of apoptosis, growth factors and cytokine production, immune and inflammatory reactions [5, 6]. In mammalian cells, NF-κB signaling system consists of homo- or heterodimers comprising at least five members – RelA (p65), RelB, c-Rel, p50/p105 (NF-κB1) and p52/p100 (NF-κB2). All NF-κB family members share a highly conserved Rel homology domain (RHD) that is responsible for binding to κB-site consensus sequence. In the resting cells, NF-κB proteins are retained inactive in the cytosol by binding to inhibitory proteins known as IκB, which are composed of multiple ankyrin (ANK) repeat domains [7, 8]. Most of IκB proteins have 6-7 ANK repeats that each consists of 33 amino acid residues and forms antiparallel α-helices separated by a loop. This family of proteins include cytoplasmic canonical IκB proteins, known as IκBα, IκBβ and IκBε, which are present in the cytoplasm of unstimulated cells and undergo stimulus-induced degradation; precursor proteins, p100 and p105, which can form the NF-κB family members p52 and p50, respectively, through their N-terminal segments; and nuclear IκBs IκBζ, Bcl-3 and IκBNS, which are absent in resting cells and induced upon cell stimulation [9, 10].

Classical (or canonical) NF-κB signaling pathway is shown in **Fig. 1**. Many different stimuli, such as pro-inflammatory cytokines, tumor necrosis factor α (TNFα), interleukin-1β (IL-1β), or Toll-like receptor (TLR) ligands activate the classical NF-κB pathway and recruit receptor proximal adaptor proteins signaling to IκB kinase complexes (IKK).

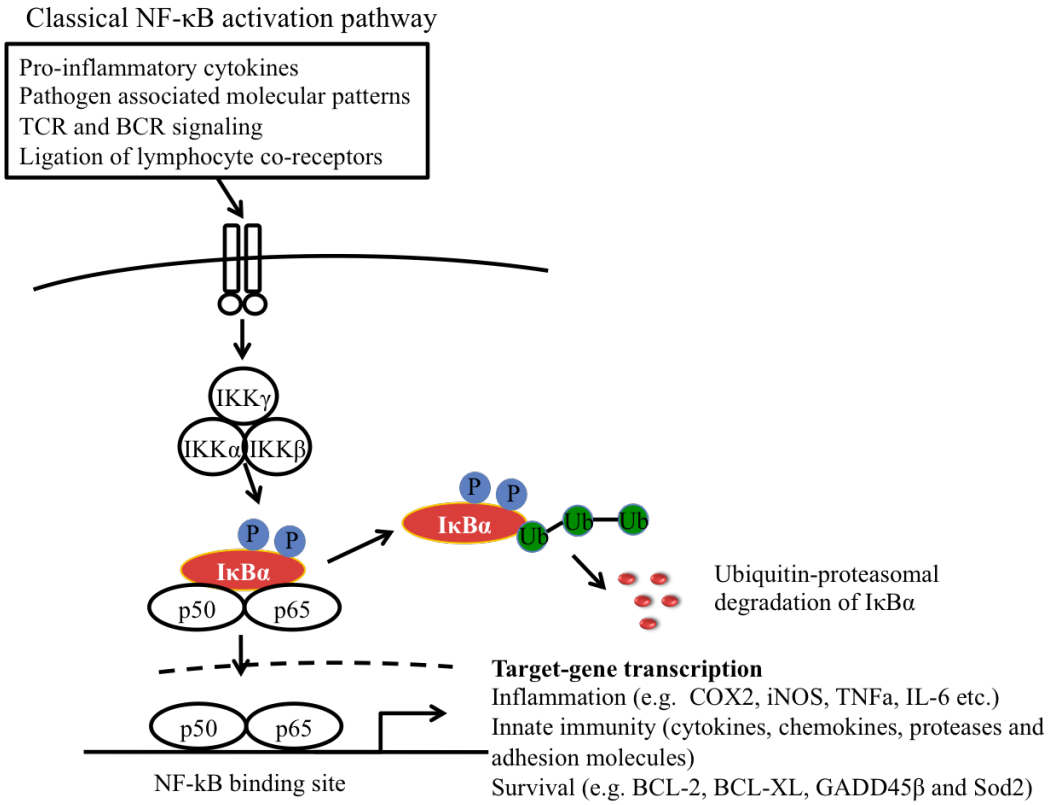


**Fig. 1. Classical (or canonical) NF-κB signaling pathway**. NF-κB dimers such as p50/p65 are maintained in the cytoplasm by interaction with inhibitory IκB molecules (often IκBα). Binding of a ligand to a cell surface receptor (e.g., TNFα or a TLR) recruits adaptors (e.g., TRAF and RIP) to the cytoplasmic domain of the receptor. In turn, these adaptors recruit an IKK complex onto the cytoplasmic adaptors (e.g., by ubiquitin-binding activity of NEMO). Activated IKK then phosphorylates IκBα at two serine residues, which leads to its ubiquitination at two lysine residues and degradation by the proteasome. NF-κB then translocates to the nucleus to activate target genes including IκBα for auto-regulation.

IKK (essentially through IKKβ) in turn phosphorylates IκBα at serine 32 and 36, leading to polyubiquitination of lysine 21 and 22 by β-TrCP containing Skp1-Culin-Roc1/Rbx1/Hrt-1-F-box (SCF) E3 complexes and subsequent degradation by the 26S proteasome [11-13]. IκBα degradation unmasks nuclear localization segment (NLS) of NF-κB and allows released dimers to translocate into the nucleus and activate target genes [14]. Classical RelA/p50 heterodimers are predominantly regulated by IκBα.

IκBα regulation on NF-κB transcription factor is very critical and misregulation of these proteins results in many different diseases [15]. For example, continuous activation of NF-κB is observed in many types of cancers and malfunction of IκBα is associated

with Hodgkin's lymphomas [16].

IκBα is composed of a N-terminal region where the phosphorylation and ubiquitination occur; ANK repeats, which bind to NF-κB, and C-terminal PEST sequence rich with proline, glutamic acid, serine and threonine residues [17, 18]. Moreover, this acidic PEST motif has been shown to be crucial for interactions with NF-κB dimer and its subsequent removal from DNA [19-21]. ANK 5 and 6 of IκBα are weekly folded and very dynamic, but they fold once bound to NF-κB [22-24]. In contrast to stability in NF-κB-bound state, free IκBα is intrinsically unstable protein with half-life of less than 10 min. It was shown that basal degradation pathways of both free and bound IκBα occur through the same signaling pathway without IKK phosphorylation, the C-terminal PEST sequence or poly-ubiquitination [25]. However, contrary to these findings, another study showed that degradation of bound IκBα did not require IKK phosphorylation but require ubiquitination. Moreover, this work demonstrated that ubiquitination is necessary for the degradation of free IκBα [26]. Free IκBα turnover was demonstrated to involve casein kinase II mediated phosphorylation preferentially at C-terminal serine 293 and subsequent ubiquitination [27], but others reported that this occurs in signal-induced degradation of bound IκBα [28] and ubiquitination is not required [29, 30]. These distinct degradation mechanisms for free and bound IκBα appear to be critical for signal-induced NF-κB activation. Giving these contradictory results in the literature and the biological significance of IκBα, I aimed to construct fusion proteins comprising full-length or fragments of human IκBα and fluorescent protein mKO2 (mKO2-IκBα) to study signal-induced degradation kinetics of IκBα. I also generated fluorescent fusion proteins with mutant IκBα to identify the involvement of different regions of IκBα such as particular ANK repeats or PEST sequence in degradation process.

Fluorescent fusion protein technology and live cell imaging have provided the opportunity to observe intracellular events, to obtain spatial and temporal information of organelles and molecules, to conduct non-invasive assessments of molecular dynamics in living cells. It also allows for quick screening of new biological drug candidates. Recently, several works have utilized fluorescent proteins to track and report the dynamics of NF-κB. Pro-inflammatory stimuli such as TNFα or hydrogen peroxide caused GFP labeled p105 to translocate to the nucleus in 20 minutes [31]. Fusion protein

of IκBα-EGFP was shown to be rapidly degraded upon TNFα or phorbol myristate acetate triggered NF-κB activation. Fluorescence resonance energy transfer (FRET) was used to analyze the interaction between p65 and IκBα using GFP proteins with dual fluorescence properties [32]. EGFP labeled p65 fusion construct was used to investigate the kinetics of NF-κB pathway in living cells upon the IL-1β stimulation [33]. The expression levels of p65-EGFP was influencing factor for the kinetics of the response to the IL-1β stimulation as well as for the NF-κB-promoted anti-apoptotic effect. This fusion construct in addition to IκBα was also used to investigate the shuttling mechanism of these proteins between nucleus and cytoplasm [34]. Recent study applied fluorescence imaging of p65 and IκBα in combination with luminescence imaging of NF-κB transcription process to investigate real-time kinetics of the NF-κB dependent transcription. Recently, Sakaue-Sawamo et al. fused fluorescent protein with the optimal fragment of the cyclin-dependent kinase inhibitor p27, which degrades through ubiquitin-proteasome pathway in cell cycle dependent manner [35]. They demonstrated that the fusion protein degraded in cell cycle dependent manner. Although much has been clarified about the biochemistry of this signaling pathway, it is unclear what factors are responsible to the kinetics and endurance of the degradation process. To address this, it is of practical importance to develop sensitive tools to visualize the signaling pathway in real-time in living cells. In addition, I used computational approach to evaluate the effect of IκBα mutations in NF-κB binding and degradation.

# Chapter I

# Design and construction of fusion proteins composed of fluorescent mKO2 and IκBα variants

## I.1 Materials and Methods

### I.1.1 Vector constructions

Fluorescent protein mKO2 (MBL) was PCR amplified using primers containing 5'NheI (GGAACCGCTAGCATGGTGAGTGTGATTAAACC) and 3'KpnI (AGAAGATGCAGTAGCTCATTGGTACCGCGGTA) sites, and digested products were cloned in-frame into the NheI/KpnI sites of pcDNA3.1 (Invitrogen) vector to generate pcDNA3.1-mKO2. The GS linker (GGGGSx3; PBS-coupler1, Riken Bioresource Center) was amplified using primers containing 5'KpnI (AAAGGTACCAACCCCTCGAGGTCGACGGTAT) and 3'XbaI (TTGCTCTAGAACTAGTGGATCCCCCGGGCT) sites, and digested products were cloned in-frame into KpnI/XbaI sites of pcDNA3.1-mKO2 to generate pcDNA3.1-mKO2-GS. The entire or numerous fragments of cDNA species of human IκBα (Gene ID: 4792, Clone ID: RDB 6668, Riken) were amplified using primers containing 5'-EcoRI (AATTAAGAATTCTTCCAGGCGGCCGAGCGCC) and 3'-BamHI (TGTAGGATCCTGCACTCATAACGTCAGACGCTG) for IκBα full length, 3'-BamHI (AGCAGCTCACCGAGGACGGGGGATCCATAATT) for IκBα (1-74 aa), 3'-BamHI (GCTGTGATCCTGAGCTCCGAGGATCCGCAT) for IκBα (1-140 aa) probes sites, and digested products were cloned in-frame into the EcoRI/BamHI sites of pcDNA3.1-mKO2-GS to generate pcDNA3.1-mKO2-GS-IκBα, pcDNA3.1-mKO2-GS-IκBα74 (IkBα1-74 aa), pcDNA3.1-mKO2-GS-IκBα140 (IκBα1-140 aa). PEST domain was amplified using primers containing 5'BamHI (AATTGGATCCCAGATGCTGCCAGAGAGTGA) and 3'XbaI (GCCAGCGTCTGACGTTATGATCTAGAGGAA) sites, and digested products were cloned in-frame into the BamHI/XbaI sites of pcDNA3.1-mKO2-GS. Then fragments of cDNA species of human IκBα were amplified using primers containing 5'EcoRI (AATTAAGAATTCTTCCAGGCGGCCGAGCGCC) and 3'BamHI (AGCAGCTCACCGAGGACGGGGGATCCATAATT) sites without stop codons, and digested products were cloned in-frame into the EcoRI/BamHI sites of pcDNA-mKO2-GS-PEST between GS and PEST, to generate pcDNA3.1-mKO2-GS-IκBα74-PEST (IkBα74-PESTΔANK1-6) and pcDNA3.1-mKO2-GS-IκBα140-PEST (IkBα140-PESTΔANK3-6) probes.

Human IκBα sequence without PEST region 277 amino acids was amplified using primers containing 5‘EcoRI (AATTAAGAATTCTTCCAGGCGGCCGAGCGCC) and 3’BamHI (GGCCGGATCCTTAAAGGTTTTCTAGTGTCAGCTGG) with added stop codon to generate pcDNA3.1-mKO2-GS-IκBα277(ΔPEST).

Colonies were screened for constructs via colony PCR followed by DNA sequencing. DNA from positive clones was purified using the Promega MiniPrep Kit according the manufacturer’s protocol.

### I.1.2 Cell culturing and transfections

HeLa cells (Riken Bioresource Center) were seeded one day before transfection at a density of $1.5\times10^4$ cells per well onto 8-well glass slide in 250 µl of complete growth medium (DMEM + 10% Fetal Bovine Serum) under humidified atmosphere at 37°C, 5% CO2, and reached 50–60% confluency at the time of transfection. Cells were transfected with plasmids using the FuGENE 6 transfection reagent (Roche Molecular Biochemicals) according to the instructions of the manufacturer (FUGENE6 transfection reagent (µl) : pDNA (µg) = 3:1).

### I.1.3 Cell fixation

Forty-eight hours post transfection, cells were washed 3 times with PBS and fixed with 4% paraformaldehyde at room temperature for 15 min and subjected to microscopy.

### I.1.4 Fluorescence microscopy

Fixed cells were visualized using Nikon Eclipse Ti inverted microscope equipped with A1R MP multiphoton confocal system (Nikon Instruments Inc., Tokyo, Japan). Images were processed with NIS-Elements AR acquisition and analysis software (Nikon Instruments Inc., Tokyo, Japan). Final arrangement of all images was performed using ImageJ software (National Institutes of Health, MD).

### I.1.5 Western blotting

HeLa cells were grown to confluence in a 100 mm culture dish in 10% FBS/DMEM and were transiently transfected and cultured as described above. Forty-

eight hours after transfection, cells were washed with PBS. Cytosol and nuclear extracts were prepared using the Nuclear Extract Kit (Active Motif), subjected to SDS-PAGE and transferred onto PVDV membrane (GE Healthcare). Membranes were probed with anti-mKO2 (PM051, MBL) antibodies. Proteins were detected with goat-anti-rabbit IgG-HRP (sc-2004 Santa Cruz Biotechnology). Chemiluminescence was developed using Luminata Western Chemiluminescent HRP Substrates. Blots were visualized using ImageQuant LAS 4000 (GE Healthcare).

## I.2 Results and Discussion

### I.2.1 Development of degradable full length and partially modified mKO2-IκBα fusion proteins

I constructed several vectors comprising fragments as well as full-length of human IκBα protein fused to mKO2.

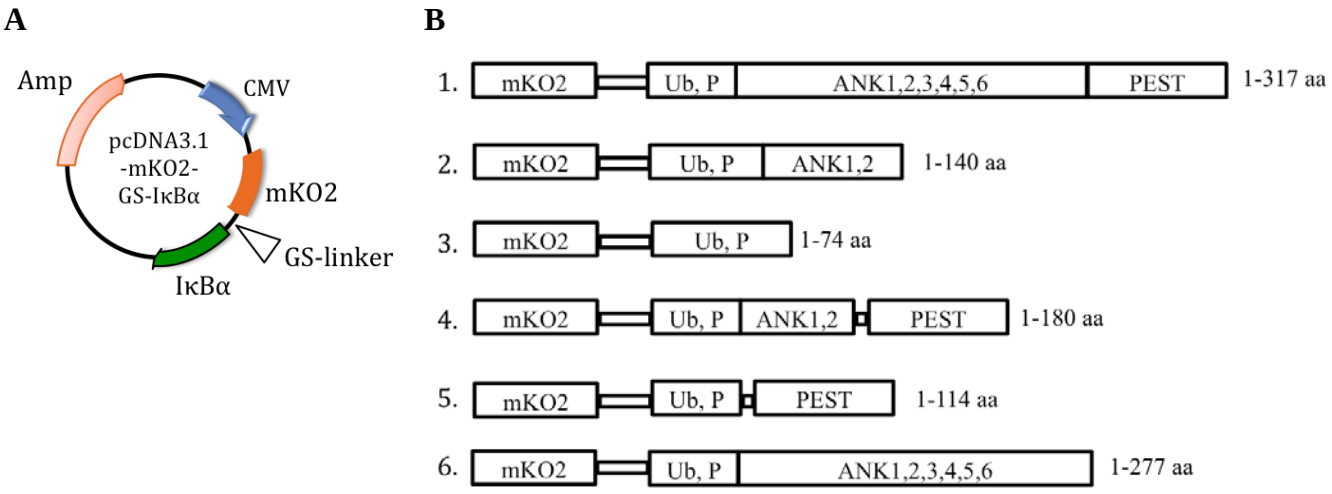


**Fig. 2. Construction of various mKO2-IκBα expression vectors.** A) Schematic outline for the construction of vector pcDNA3.1-mKO2-GS-IκBα. B) Overall strategy for development of fusion proteins with fragments of IκBα protein (for description see Table 1). Amp, ampicillin resistance gene; CMV, cytomegalovirus promoter; mKO2, monomeric Kusabira orange 2 gene; IκBα, human inhibitor of NF-kappa B alpha gene; PEST gene, sequence of proline, serine, threonine, aspartate, and glutamate residues; ANK, ankyrin repeat domain; Ub, P, ubiquitination and phosphorylation domain.

As fragments of IκBα, I chose three domains: N terminal phosphorylation and ubiquitination domain (amino acids 21-36), ANK repeats 1 and 2 that are responsible for NF-κB binding (amino acids 73-139) and C terminal PEST domain (amino acids 277-317). These domains were fused to mKO2 with GS linker in different combinations. Design of total six constructs is shown in **Fig. 2**. A nomenclature and description of vector constructs are shown in **Table 1**.

**Table 1. Nomenclature and description of constructed vectors.**

| | Fusion protein name | Description |
|---|---|---|
| 1 | mKO2::IκBα | mKO2 fused to full length IκBα containing PEST domain |
| 2 | mKO2::IκBα140(IκBαΔANK3-6,PEST) | mKO2 fused to N terminal ubiquitination-phosphorylation domain of IκBα lacking ANK repeats 3, 4, 5, 6 and PEST domain. |
| 3 | mKO2::IκBα74(IκBαΔANK1-6,PEST) | mKO2 fused to N terminal ubiquitination-phosphorylation domain of IκBα lacking all six ANK repeats and PEST domain. |
| 4 | mKO2::IκBα140-PEST(IκBαΔANK3-6) | mKO2 fused to N terminal ubiquitination-phosphorylation domain of IκBα lacking ANK 3, 4, 5, 6 repeats. |
| 5 | mKO2::IκBα74-PEST(IκBαΔANK1-6) | mKO2 fused to N terminal ubiquitination-phosphorylation domain of IκBα lacking all six ANK repeats. |
| 6 | mKO2::IκBα277(IκBαΔPEST) | mKO2 fused to full length IκBα lacking PEST domain. |

A PCR product comprising the DNA sequence, which encoded the mKO2 (651 bp) was derived from PCR amplification and cloned into the pcDNA3.1 vector. Cloning was confirmed by Colony PCR as shown in **Fig. 3** and sequencing (data not shown). Next GS linker (GGGGS)3x was amplified and cloned into pcDNA3.1-mKO2 vector. Cloning was confirmed by colony PCR and result is shown in **Fig. 4**.

To clone full length or fragments of human IκBα protein, primers were picked up without start codon to ensure that the final protein will be expressed as a single fusion protein. For mKO2::IκBα fusion protein full length IκBα was amplified and cloned into

pcDNA3.1-mKO2-GS. For mKO2::IκBα140(IκBαΔANK3-6,PEST) fusion protein N terminal 140 amino acid was amplified and cloned into pcDNA3.1-mKO2-GS. This fusion protein lacks ANK repeats 3,4,5,6 and C terminal PEST region of human IκBα. To generate mKO2::IκBα74(IκBαΔANK1-6,PEST) fusion protein N terminal 74 amino acid was amplified and digested products were cloned into pcDNA3.1-mKO2-GS.

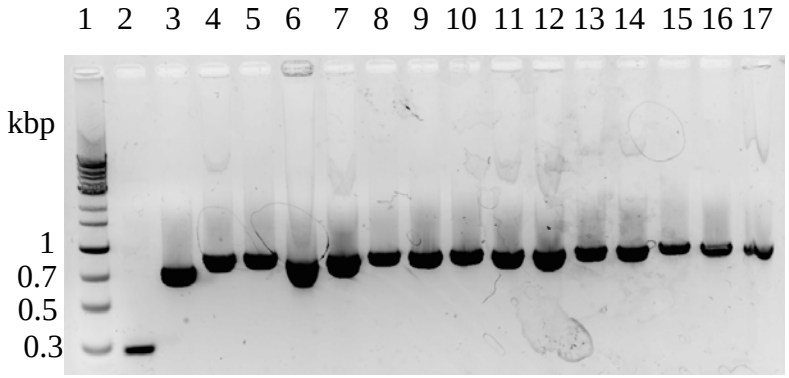


**Fig. 3. Colony PCR results of mKO2 protein cloning region.** The PCR products were electrophoresed on a 1.2% agarose gel containing Green Gel Wako at a final concentration of 0.02% (v/v). Lane 1 Marker 1 kbp (Nakalai); 2 Negative control (no DNA); 3 PCR positive control: original cloning vector insert size 678 bp. Colony PCR primers T7,BGH specific for pcDNA3.1. 4,5,8-17 positive colonies insert size 813 bp.

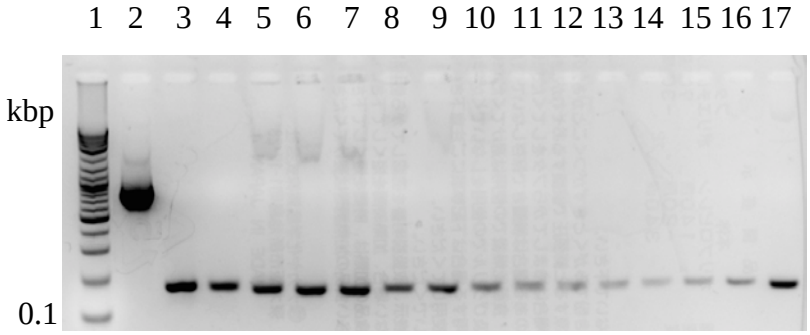


0.5

**Fig. 4. Colony PCR analysis of positive mKO2::GS clone colonies.** The PCR products were electrophoresed on a 1.2% agarose gel containing Green Gel Wako at a final concentration of 0.02% (v/v). Lane 1 Marker Broad Range (Nakalai); 2 PCR positive control Marker 1: colony PCR vectors for pcDNA3.1 T7,BGH; 3 PCR positive control for insert using same primers as in PCR amplification. 4-7, 17 positive colonies, insert size 125 bp.

This fusion protein lacks all six ANK repeats and C terminal region of human IκBα. Stop codons were inserted to the reverse primers for PCR amplification of fragments of

human IκBα. Colony PCR results for cloning mKO2::IκBα, mKO2::IκBα140(IκBαΔANK3-6,PEST) and mKO2::IκBα74(IκBαΔANK1-6,PEST) are shown in **Fig. 5**.

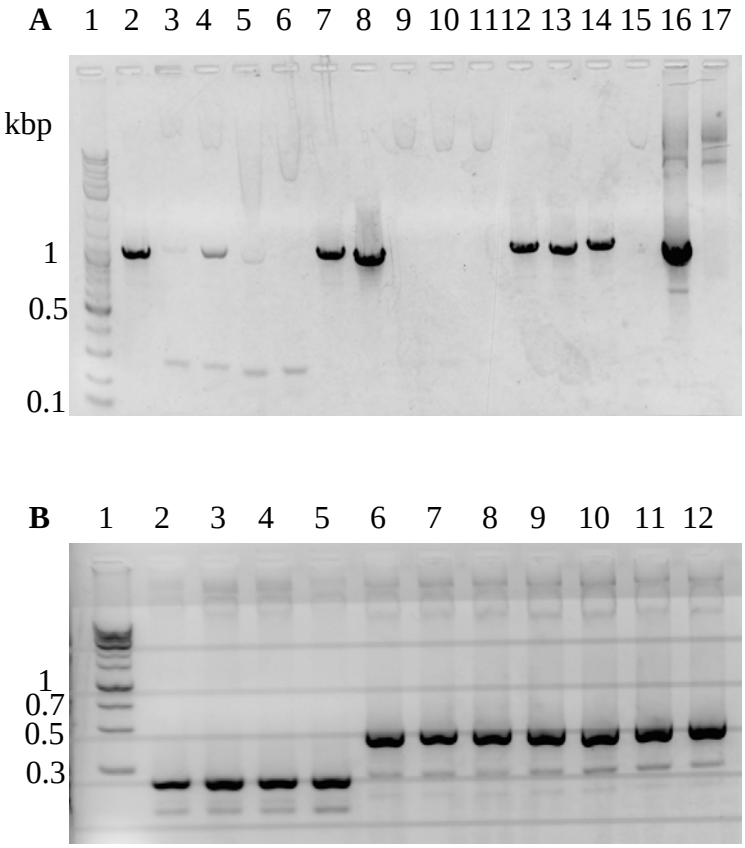


**Fig. 5. Colony PCR analysis of (A) mKO2::IκBα (full length), (B) mKO2::IκBα74(IκBαΔANK1-6,PEST) and mKO2::IκBα140(IκBαΔANK3-6,PEST) colonies.** The PCR products were electrophoresed on a 1.2 % agarose gel containing Green Gel Wako at a final concentration of 0.02% (v/v). A: lane 1 Marker 1 kbp (Nakalai); 2 Positive control; 3 Negative control; 7,8, 12-14 positive colonies insert size 956 bp. B: lane 1 Marker 1 kbp DNA ladder One (Nakalai); 2-5 positive colonies of mKO2-GS-IκBα74 insert size 250 bp; 6-12 positive colonies of mKO2-GS-IκBα140 insert size 420 bp.

I observed that proteins mKO2::IκBα140(IκBαΔANK3-6,PEST) containing phosphorylation-ubiquitination domain and ANK repeats 1-2, and mKO2::IκBα74(IκBαΔANK1-6,PEST), which lacks ANK repeats 1-2 but contains only N-terminal phosphorylation-ubiquitination domain did not degrade upon pro-

inflammatory activation in HeLa cells (see Chapter II). I hypothesized that PEST might be required independently from ANK repeats for stimulus-induced degradation.

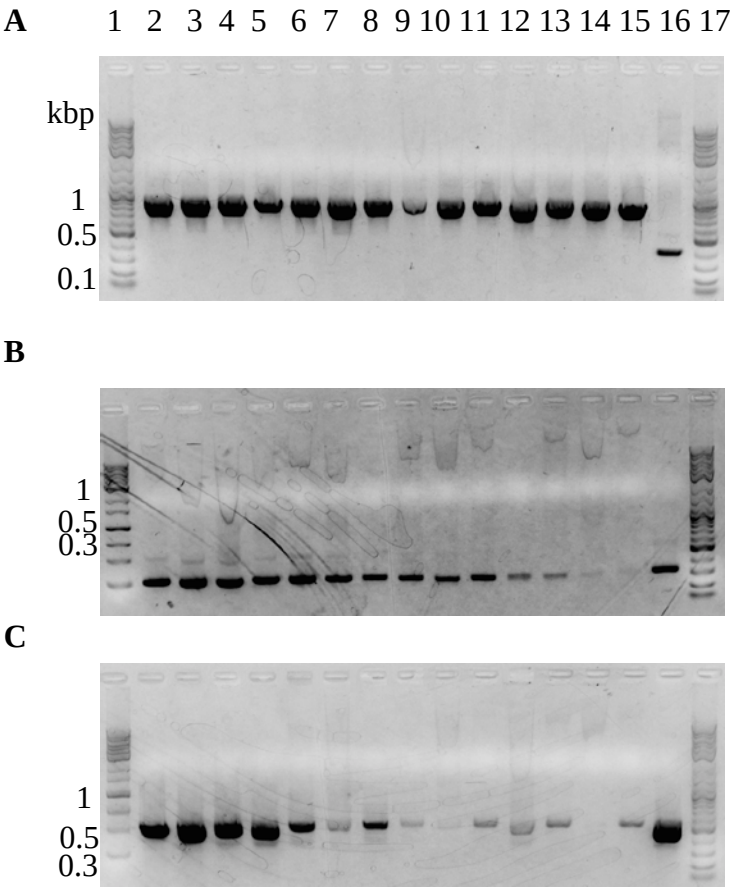


**Fig. 6. Colony PCR analysis of mKO2::GS::PEST (A), mKO2::IκBα74-PEST(IκBαΔANK1-6) (B) and mKO2::IκBα140-PEST(IκBαΔANK3-6) (C) clones.** The PCR products were electrophoresed on a 1.2 % agarose gel containing Green Gel Wako at a final concentration of 0.02% (v/v). A: lane 1, 17 Marker Broad Range (Nakalai); 2-8 and 10-15 positive colonies. Colony PCR primers used: F-TGGCTAGCATGGTGAGTGTG, R- GCTCGTCCTCTGTGAACTCC. Primers were generated with online software Primer3 Plus. Insert size 849 bp. B: lane 1 Marker 1 kbp (Nakalai); 2 positive control PCR sample; 3-11, 16 positive colonies; 17 Marker Broad Range (Nakalai). Insert size 310 bp. Primers were the same as used for PCR amplification. C: lane 1 Marker 1 kbp (Nakalai); 2 positive control; 3-6,8,16 positive colonies; 17 Marker Broad Range. Insert size 417 bp; Colony PCR primers were the same as used for amplification.

Therefore, to test this hypothesis I fused 40 amino acids PEST domain to the C-terminal of fusion proteins comprising fragments of IκBα to generate mKO2::IκBα74-PEST(IκBαΔANK1-6) and mKO2::IκBα140-PEST(IκBαΔANK3-6).

C terminal 40 amino PEST region of human IκBα was cloned in-frame into the BamHI/XbaI sites of pcDNA3.1-mKO2-GS to generate pcDNA3.1-mKO2-GS-PEST (**Fig. 6 A**). Then fragments of cDNA species of human IκBα 1-74 aa and IκBα 1-140 aa without start codons were cloned in-frame into the EcoRI/BamHI sites of pcDNA3.1-mKO2-GS-PEST between GS and PEST sites to generate mKO2::IκBα74-PEST(IκBαΔANK1-6) (**Fig. 6 B**) and mKO2::IκBα140-PEST(IκBαΔANK3-6) (**Fig. 6 C**) probes respectively. Subsequently, cloning was confirmed by colony PCR and DNA sequencing (**Fig. 6** and data not shown).

For construction of vector with full-length IκBα, which lacks the PEST domain, fragment of cDNA species of human IκBα (IκBα 1-277 aa) with added stop codon were cloned in-frame into the EcoRI/BamHI sites of pcDNA3.1-mKO2-GS to generate mKO2::IκBα277(IκBαΔPEST) protein (**Fig. 7).**

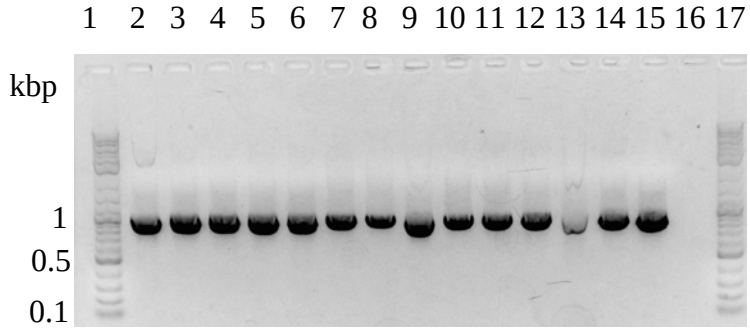


**Fig. 7. Colony PCR analysis of positive mKO2::IκBα277(IκBαΔPEST) clone colonies.** The PCR products were electrophoresed on a 1.2 % agarose gel containing Green Gel Wako at a final concentration of 0.02% (v/v). Lane 1 and 17 Marker Broad Range (Nakalai); 2 positive control; 3-12, 14, 15 positive colonies. Insert size 828 bp.

### I.2.2 Observation of fluorescence intensity in HeLa cells expressing mKO2-IκBα

All fusion proteins expressed well in transfected HeLa cells as confirmed by fluorescence microscopy and western blotting (**Fig. 8**). Constructed vectors were transiently transfected into HeLa cells followed by the fixation and imaging by fluorescence microscopy. Fusion proteins were mainly expressed in cytoplasm. In

unstimulated cells expressing mKO2::IκBα, strong red fluorescence signal localized in cytoplasm and nucleus was readily observed under the microscope. The strongest intensity was obtained with the transfection efficiency above 60 % when cells were kept at 37°C for 24 h after removing the transfection complex and then incubating cells at 37°C for another 36-48 hr. It is seen in **Fig. 8** that mKO2 appears to be distributed throughout the cytoplasm. Identical pattern was observed in cells expressing fusion constructs and was confirmed by western blot analysis (for degradable proteins).

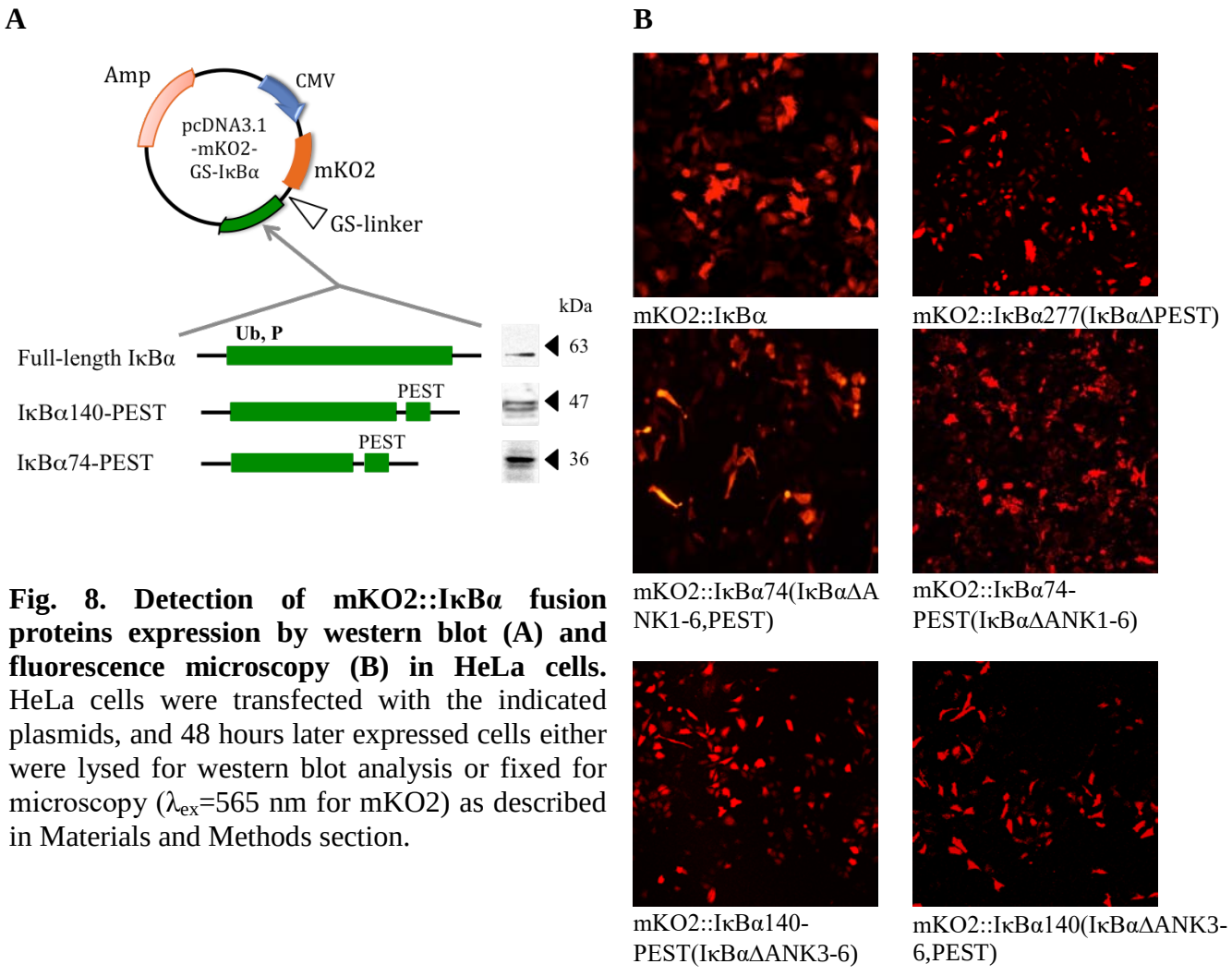


**Fig. 8. Detection of mKO2::IκBα fusion proteins expression by western blot (A) and fluorescence microscopy (B) in HeLa cells.** HeLa cells were transfected with the indicated plasmids, and 48 hours later expressed cells either were lysed for western blot analysis or fixed for microscopy ($\lambda_{ex}$=565 nm for mKO2) as described in Materials and Methods section.

## I.3 Conclusion

Novel constructs to monitor the behavior and dynamics of IκBα protein were developed. The strategy involves the construction of six novel expression vectors, in which the mKO2 gene was fused to full-length or fragments of human IκBα. Three domains of IκBα, i.e., N-terminal phosphorylation and ubiquitination domain, ANK repeats 1 and 2, and C-terminal PEST domain, were fused to mKO2 with amino acid linker $(GGGGS)_3$ (GS linker) in different combinations to construct mKO2::hIκBα, mKO2::IκBα140(IκBαΔANK3-6,PEST), mKO2::IκBα74(IκBαΔANK1-6,PEST), mKO2::IκBα140-PEST(IκBαΔANK3-6), mKO2::IκBα74-PEST(IκBαΔANK1-6) and mKO2::IκBα277(IκBαΔPEST). Results of western blot and sequencing confirmed the expression of these vectors. All constructed vectors were confirmed to be effectively expressed *in vitro* in transfected HeLa cells as demonstrated by the appearance of the fluorescence signal of mKO2. The constructed fusion proteins were suggested to serve as the potential tool for analysis of IκBα protein dynamics.

# Chapter II
# Real-time imaging and analysis of degradation kinetics of IκBα using mKO2 fusion proteins in living cells

## II.1 Materials and Methods

### II.1.1 Cell culture and transfection

HeLa cells were cultured in DMEM with 10% FBS and maintained at 37°C, 5% $CO_2$. For confocal microscopy, cells were plated in 35 mm glass-bottom dishes (Iwaki) at $5 \times 10^4$ cell/mL in 2 ml medium. After 24 h, cells were transfected with appropriate plasmids using FuGENE 6 (Roche) with optimized ratio reagent:DNA of 3:1. Forty-eight hours post transfection, cells were washed 3 times with PBS and the medium was replaced with Opti-MEM® without phenol red (Invitrogen) and stimulated with 10 ng/mL TNFα (Calbiochem).

### II.1.2 Time-lapse confocal imaging

Confocal microscopy was carried out on transfected cells in 35 mm glass-bottom dishes under the Nikon A1RMP Multiphoton Confocal Microscope (Nikon Instruments Inc.) maintaining humidified conditions by stage top incubator (Tokai Hit) at 37°C and 5% $CO_2$ using 10× or 20× Plan Apo objective lenses. mKO2 was exited at 561 nm. Data was recorded and processing was carried out using built-in NIS Elements software (Nikon Instruments Inc.) and Image J (National Institutes of Health, MD). For fusion proteins, mean cellular fluorescence intensities were calculated at each time point, and fluorescence intensity relative to starting fluorescence signal was detected for each cell.

### II.1.3 Western blotting

HeLa cells were grown to be confluent in a 100 mm culture dish in 10% FBS/DMEM and transiently transfected as described. Forty-eight hours after transfection cells were stimulated with TNFα (10 ng/mL) for indicated times and washed with PBS. Cytoplasmic extraction was performed using Active Motif Nuclear extraction kit according to the manufacturer's instruction. Total protein was quantified using Bradford Assay according to the manufacturer's instruction. Cytoplasmic fraction of cells was diluted in 2X SDS-PAGE loading buffer (0.125mM Tris-HCl, pH6.8, 4% SDS, 20% glycerol, 10% 2-Mercaptoethanol, 0.004% BPB) and denatured at 90°C for 5 min. Proteins were separated by polyacrylamide gel electrophoresis using 12,5% SuperSep Ace (Wako) and transferred to a polyvinylidene difluoride (PVDF) membrane.

Membranes were blocked overnight at 4°C in BSA 1 % Tween 20 and probed using anti-IκBα (sc-847 Santa Cruz), anti-IκBα c-21 (sc-371, Santa Cruz), anti-mKO2 (PM051, MBL) and anti-beta actin-HRP (sc-47778, Santa Cruz) antibodies. Proteins were detected with goat-anti-rabbit IgG-HRP (sc-2004, Santa Cruz). Chemiluminescence was developed using Luminata Western Chemiluminescent HRP Substrate (Millipore, Sigma).

### II.1.4 Treatment of cells with TNFα and proteasomal inhibitors

In all the experiments, the cell cultures were kept in DMEM containing 10% FBS for 24 h before the stimulations. Cells were treated with TNFα immediately before the microscopy by replacing 1/100 of the culture medium volume in the 35 mm dish with the appropriate solution to make of 10 ng/mL the final concentration. Cells were treated with lactacystin for 24 hours prior to the TNFα treatment at concentrations of 25 μM, except where otherwise indicated. DMSO 1% (v/v) was used as a vehicle for lactacystin and was run in parallel in all cases as control. A series of experiments using another inhibitor of the proteasome, MG132, were performed to compare the results obtained with lactacystin. The concentrations of MG132 used were 50 μM, and controls containing DMSO 0.25% (v/v) (the solvent used as vehicle) were run in parallel. Samples containing no additions compared with controls containing the vehicle solutions gave similar results. Each experiment was carried out at least three times with at least 10-15 cells obtained per repeat.

### II.1.5 Image analysis

Captured images were recorded at different time frames (excitation wavelength of 561 nm and an emission wavelength of 595 nm. After subtracting the background signal, the fluorescence intensity of the pixels of cells in each image was converted to inherent values for each individual cell using ImageJ 1.48v (National Institutes of Health, MD). The results are expressed as the mean ± S.D. of at least three independent cell cultures.

## II.2 Results and Discussion

### II.2.1 Visualization of TNF-α induced IκBα degradation

Exposure of cells to the pro-inflammatory stimuli such as TNFα leads IκBα to rapidly degrade by a proteolytic system that is required for nuclear translocation and activation of NF-κB [11-13]. As we better understand the regulation of the IκBα degradation, potential for inhibiting this pathway has received great attention. Agents that inhibit this pathway, such as glucocorticoids and aspirin, can reduce the inflammatory response [2]. To visualize the degradation of IκBα in the cytosol, I used constructed fusion proteins of mKO2::IκBα and studied in transfected HeLa cells by real-time confocal microscopy.

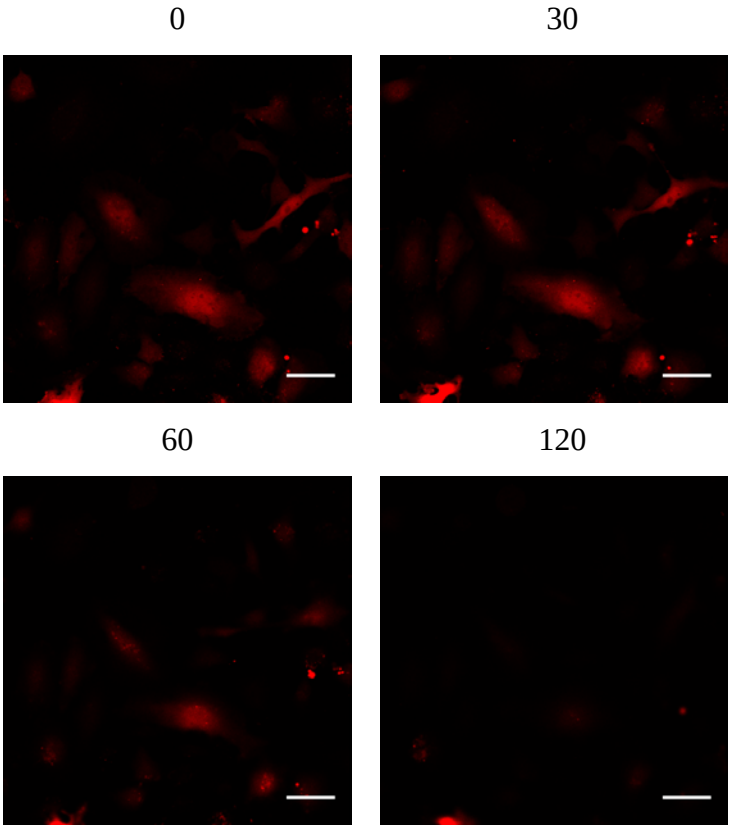


**Fig. 9. Degradation of mKO2::IκBα in response to TNFα stimulation.** Time series images of mKO2::IκBα fluorescence at indicated times (min) after addition of TNFα (10 ng/mL). Scale 50 μm.

As shown above, in unstimulated cells expressing mKO2::IκBα, cytoplasmically located stable fluorescence was observed (**Fig. 8**). In time-lapse images of cells transfected with mKO2::IκBα comprising full-length human IκBα protein, following the addition of 10 ng/mL TNFα to the culture medium, fluorescence intensity began to decrease approximately 7 minutes later (**Fig. 9**).

Fluorescence live imaging was performed within 2 hours time frame after TNFα stimulation. In contrast, decrease of fluorescence intensity was not observed in cells expressing only mKO2 fluorescent protein after TNFα stimulation (**Fig. 10**), suggesting that degradation occurs when mKO2 is fused to IκBα.

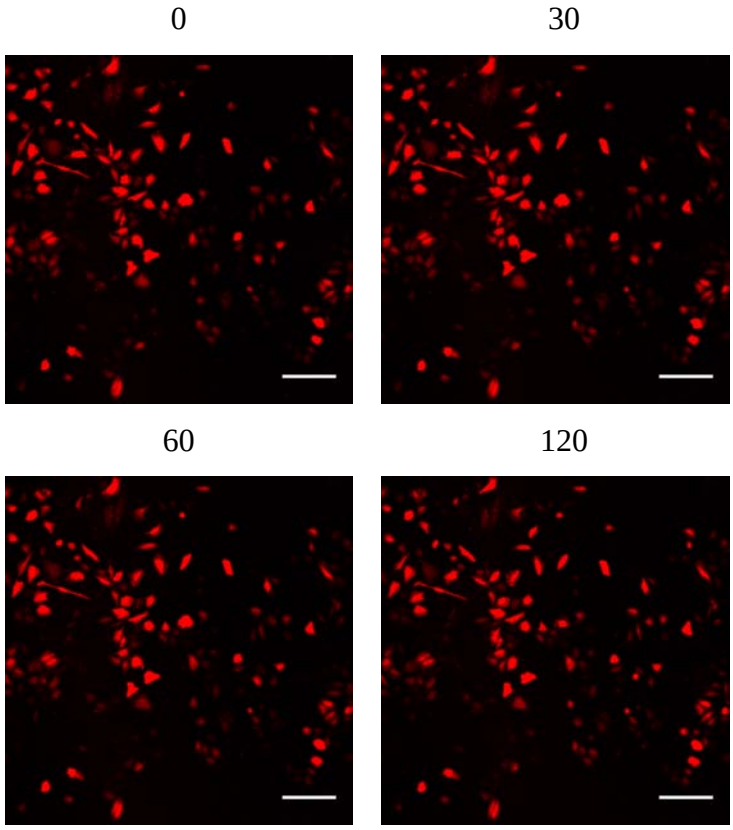


**Fig. 10**. **Fluorescence of mKO2 in response to TNFα stimulation.** Time series images of mKO2 fluorescence at indicated times (min) after addition of TNFα (10 ng/mL). Scale 100 μm.

### II.2.2 Involvement of ANK repeats in TNFα induced IκBα degradation

In order to understand how the different regions of the IκBα contribute to the signal-induced degradation process, I generated IκBα deletion mutants by removing ANK repeats and/or C-terminal PEST sequence. Structurally IκBα can be divided into three domains, N-terminal signal response region where the phosphorylation and ubiquitination occurs, six ANK repeats, ANK 1, 2 responsible for NF-κB binding and a C-terminal PEST sequence. Amino acid residues vicinal to both the p50 and p65 NLS are

restrained to the first two ANK repeats of IκBα, suggesting a mechanism for cytoplasmic retention of NF-κB [17]. First, I removed all ANK repeats leaving only N terminal phosphorylation-ubiquitination domain (mKO2::IκBα74(IκBαΔANK1-6,PEST)). There was no decay in fluorescence observed in the cells transfected with this probe (**Fig. 11A**). Next, I removed all ANK repeats except for ANK 1 and 2 (mKO2::IκBα140(IκBαΔANK3-6,PEST)). This probe did not degrade upon TNFα stimulation either (**Fig. 11B**), suggesting that responsible region for degradation lies below the ANK repeats down to C terminal.

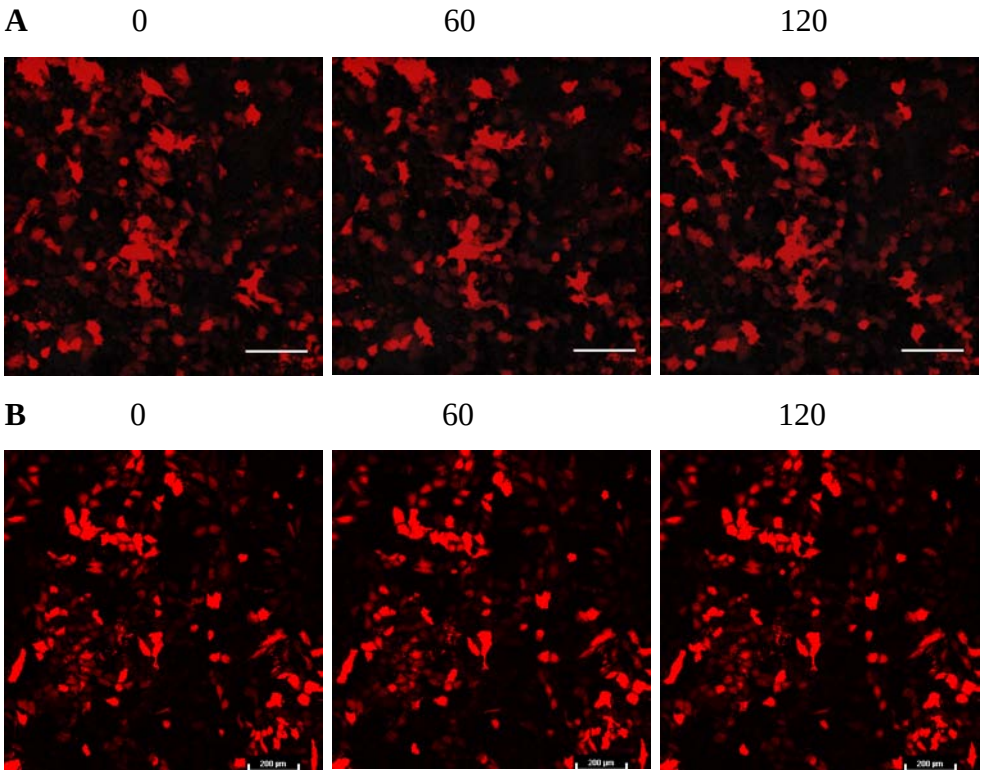


**Fig. 11**. **Fluorescence of fusion proteins with deletions of ANK repeats in response to TNFα stimulation.** Time series images of mKO2::IκBα140(IκBαΔANK3-6,PEST) (A) and mKO2::IκBα74(IκBαΔANK1-6,PEST) (B) fluorescence at indicated times (min) after addition of TNFα (10 ng/mL). Scale 200 μm.

To test this hypothesis and investigate how ANK repeats beyond the first two can potentiate the signal-induced degradation of IκBα, the cells were transfected with the expression construct comprising mKO2 fused to N-terminal phosphorylation-

ubiquitination domain and all ANK repeats from one to six (mKO2::IκBα277(IκBαΔPEST)) but lacking the PEST domain. The mKO2::IκBα277(IκBαΔPEST) showed slight decay in fluorescence intensity upon stimulation with TNFα but was not degraded (**Fig. 12**). Degradation was significantly inhibited compared with mKO2::IκBα (contains PEST domain).

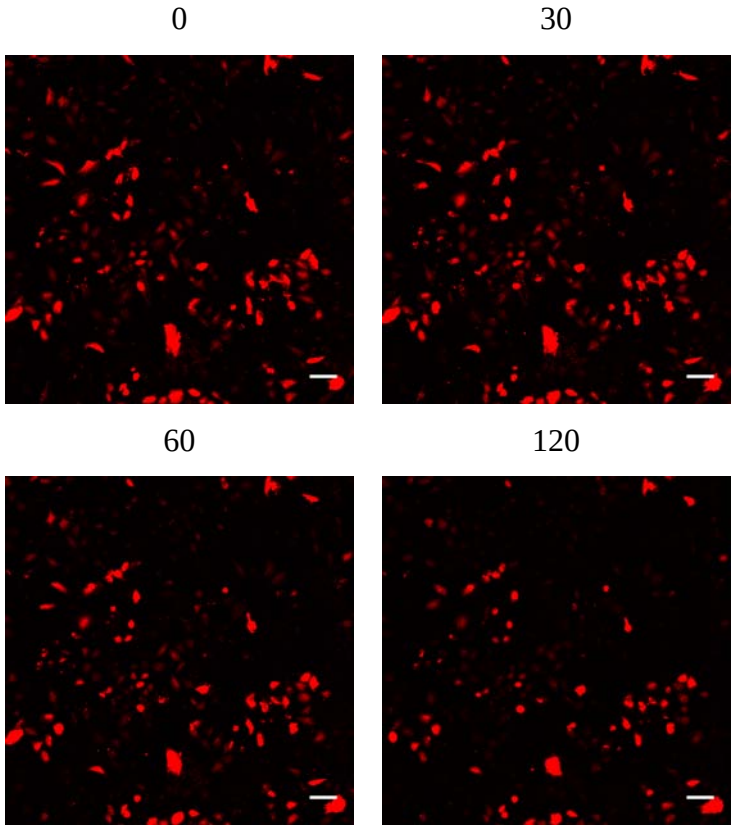


**Fig. 12. Fluorescence of mKO2::IκBα277(IκBαΔPEST) with deletions of C-terminal PEST sequence in response to TNFα stimulation.** Time series images of mKO2::IkBa277(IκBαΔPEST) fluorescence at indicated times (min) after addition of TNFα (10 ng/mL). Scale 100 µm.

### II.2.3 The role of the PEST sequence in TNFα induced IκBα degradation

Our results regarding the real-time degradation analysis of PEST lacking mutant probes i.e., mKO2::IκBα140(IκBαΔANK3-6,PEST), mKO2::IκBα74(IκBαΔANK1-6,PEST) and mKO2::IκBα277(IκBαΔPEST), imply that PEST sequence may be required for stimulus-triggered degradation of IκBα. To test this hypothesis, I generated two fusion proteins by cloning 40-amino acid PEST domain directly to the N-terminal phosphorylation-ubiquitination domain after removing all six ANK repeats

(mKO2::IκBα74-PEST(IκBαΔANK1-6)) and to ANK repeats 1, 2 (mKO2::IκBα140-PEST(IκBαΔANK3-6). As a result, clear decay in fluorescence was observed in the cells expressing both mKO2::IκBα74-PEST(IκBαΔANK1-6) and mKO2::IκBα140-PEST(IκBαΔANK3-6) about 5-7 minutes after TNFα stimulation (**Fig. 13**). Although, there are contradictory reports related to the involvement of PEST sequence in IκBα degradation [36-38], our data suggest that PEST is necessary for the signal-induced IκBα degradation. Moreover, I show that PEST sequence functions independently from ANK repeats.

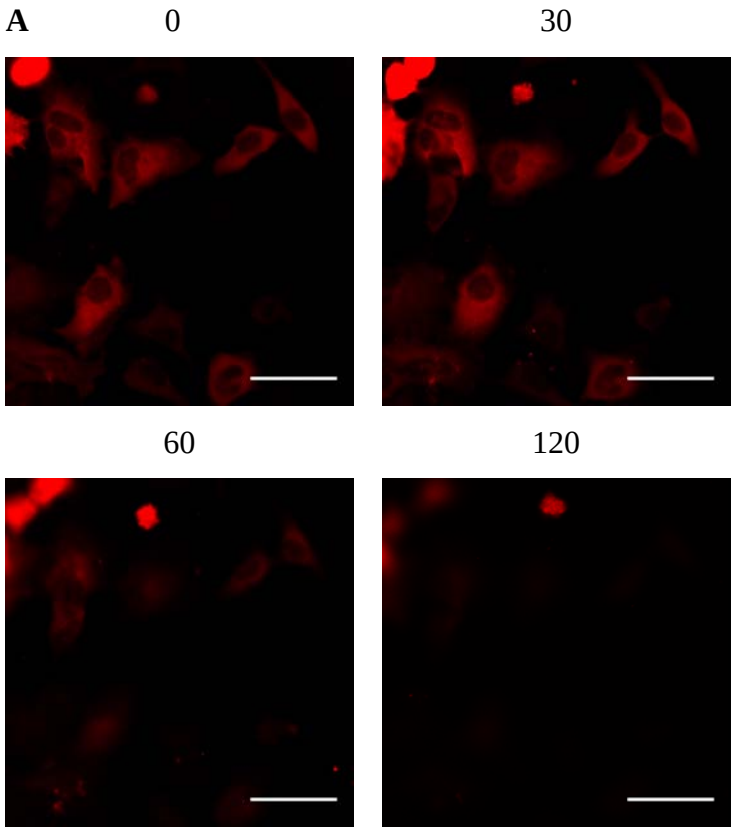

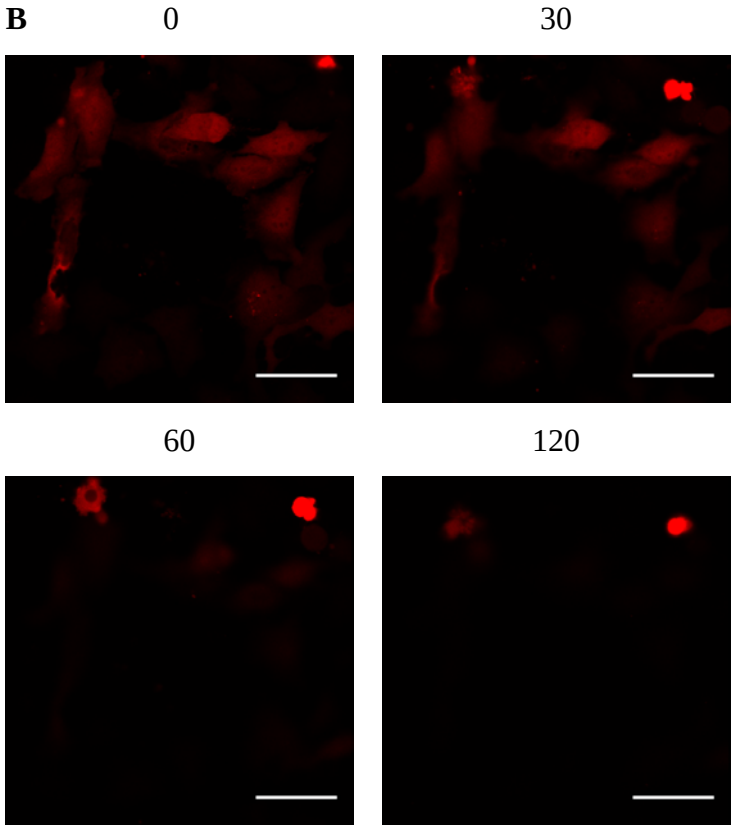


**Fig. 13**. **Effect of PEST sequence in degradation of fusion proteins.** Time series images of mKO2::IκBα74-PEST(IκBαΔANK1-6) (A) and mKO2::IκBα140-PEST(IκBαΔANK3-6) (B) fluorescence at indicated times (min) after addition of TNFα (10 ng/mL). Scale 50 μm.

Stimulus-induced degradation of mKO2::IκBα74-PEST(IκBαΔANK1-6), mKO2::IκBα140-PEST(IκBαΔANK3-6), and full-length mKO2::IκBα was also confirmed by Western blot analysis and compared with degradation of endogenous IκBα (**Fig. 14**). Each transfected cell culture was subjected to a specific stimulus followed by Western blot analysis of cytoplasmic extracts with IκBα-specific antibodies except for mKO2::IkBa74-PEST(IκBαΔANK1-6) where anti-mKO2 antibodies were used.

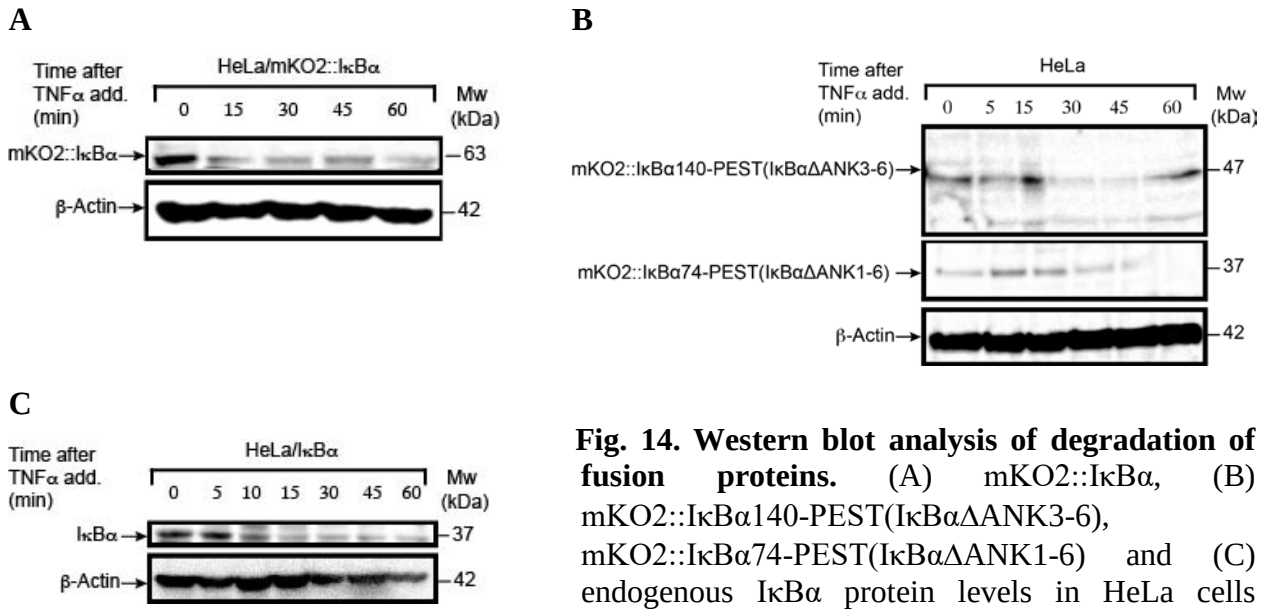


**Fig. 14. Western blot analysis of degradation of fusion proteins.** (A) mKO2::IκBα, (B) mKO2::IκBα140-PEST(IκBαΔANK3-6), mKO2::IκBα74-PEST(IκBαΔANK1-6) and (C) endogenous IκBα protein levels in HeLa cells stimulated with continual 10 ng/mL TNFα for the indicated times.

### II.2.4 Effects of lactacystin on degradation of fusion proteins

Signal-induced degradation of IκBα occurs via ubiquitin-proteasome pathway [39, 40]. Stimulation-dependent IκBα phosphorylation at serine residues 32 and 36 [41-43] targets IκBα to the ubiquitin-proteasome pathway. Then ubiquitination occurs at lysine residues 21 and 22 [44, 45] followed by the proteasomal degradation of IκBα, which allows NF-κB to be released and enter the nucleus [46-48].

To confirm whether ubiquitin-proteasome pathway is involved in degradation of fusion proteins and to evaluate the applicability of this platform to test effect of proteasomal inhibitors in degradation, I treated HeLa cells with lactacystin, an irreversible and selective 20 S proteasome inhibitor, which acts by targeting the catalytic B-subunit [49], before exposing them to TNFα.

I showed that TNFα-induced degradation was not observed in lactacystin pre-treated HeLa cells expressing fusion proteins (**Fig. 15**) suggesting that like endogenous IκBα, fusion proteins are degraded primarily via proteasomal pathway.

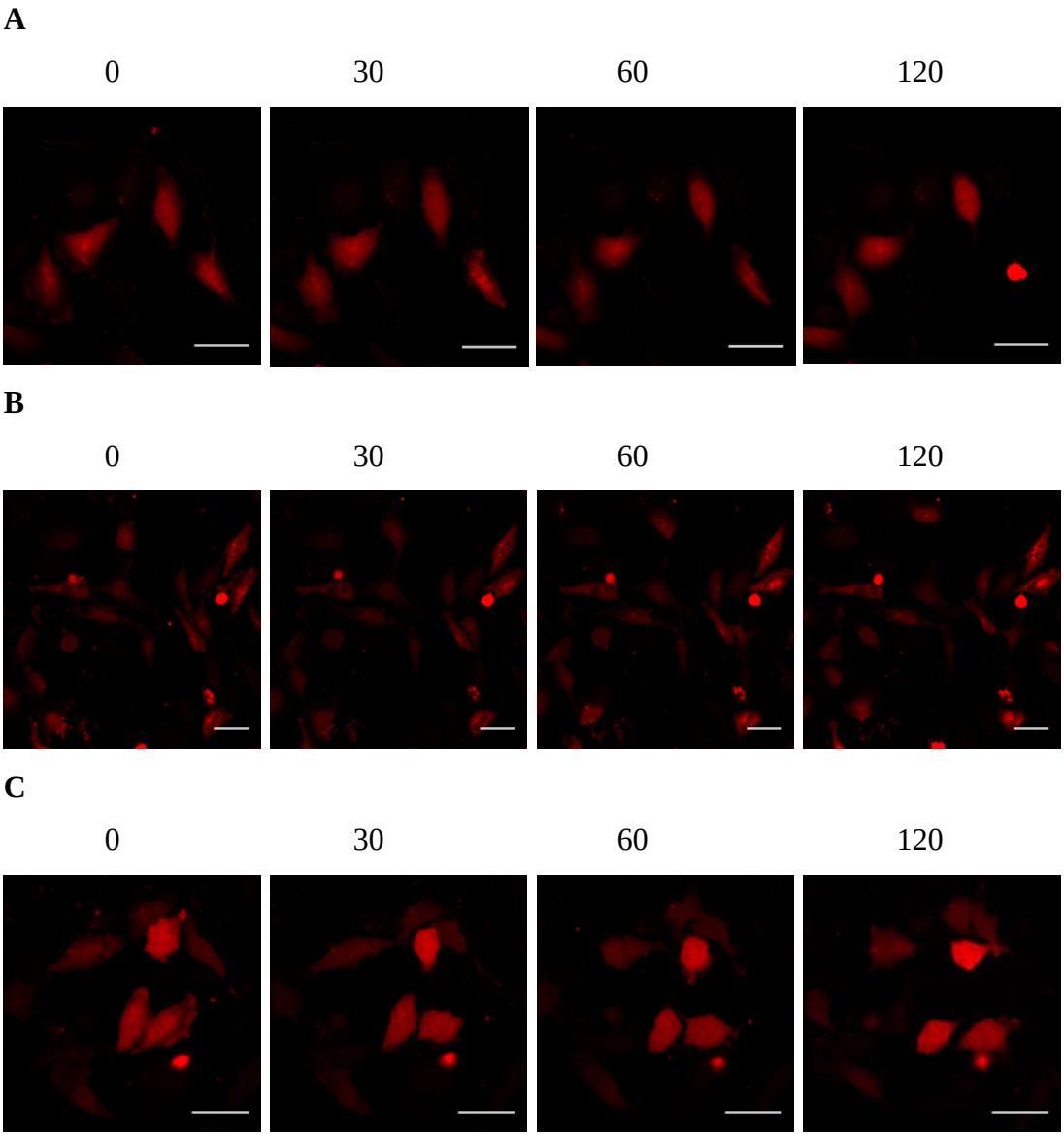


**Fig. 15. Effect of lactacystin on degradation of fusion proteins.** Time series images of (A) mKO2::IκBα, (B) mKO2::IκBα140-PEST(IκBαΔANK3-6), (C) mKO2::IκBα74-PEST(IκBαΔANK1-6) fluorescence at indicated times (min) after addition of TNFα. Degradation was prevented in cells treated with 25 μM lactacystin for 24 h prior to addition of TNFα. Scale 50 μm.

### II.2.5 Effects of the inhibition of proteasome activity by MG132

A series of experiments treating the HeLa with another inhibitor of the activity of the 26S proteasome, MG132 [50], was performed to give additional support to the results obtained using lactacystin. As expected, TNFα-induced degradation was not observed in the cells expressing fusion constructs full-length mKO2::IκBα, mKO2::IκBα140-

PEST(IκBαΔANK3-6) and mKO2::IκBα74-PEST(IκBαΔANK1-6) in the cells pretreated with MG132 (**Fig. 16**).

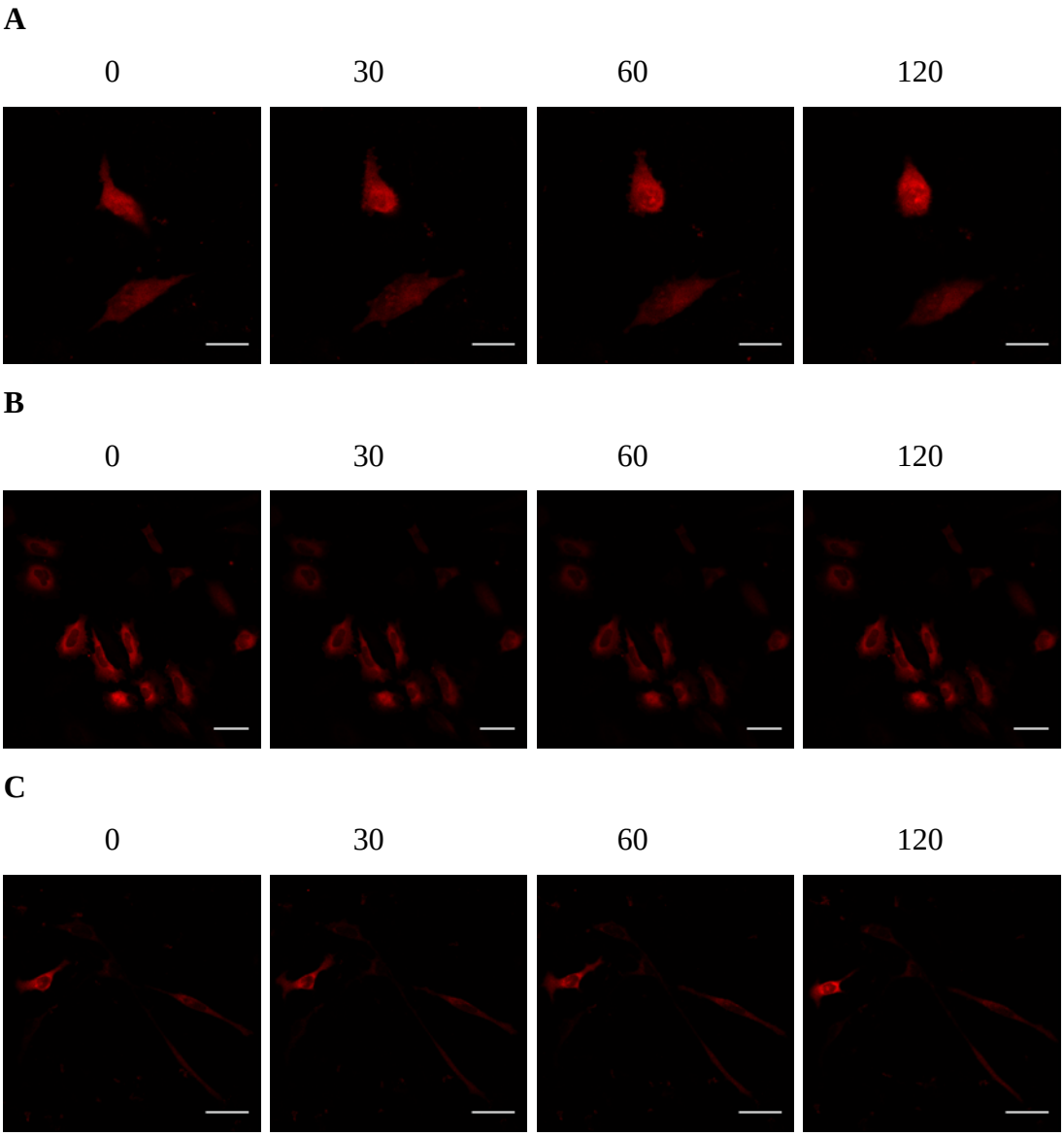


**Fig. 16. Effect of MG132 on degradation of fusion proteins.** Time series images of (A) mKO2::IκBα, (B) mKO2::IκBα140-PEST(IκBαΔANK3-6), (C) mKO2::IκBα74-PEST(IκBαΔANK1-6) fluorescence at indicated times (min) after addition of TNFα. Degradation was prevented in cells treated with 50 μM MG132 for 24 h prior to addition of TNFα. Scale 50 μm.

### II.2.6 Analysis of kinetics of IκBα degradation using fusion proteins

To investigate the kinetics of IκBα degradation, I quantitatively analyzed the decay of fluorescence of each fusion-construct over the periods of several hours following the

TNFα stimulation. Cells expressing the mKO2::IκBα fusion protein showed mainly cytoplasmic fluorescence 48 h post transfection. A rapid decay in fluorescence was observed upon stimulation with TNFα. The half-life of degradation of mKO2::IκBα full-length protein was determined by quantitative fluorescence analysis to be 37 minutes (**Fig. 17**). These observations are in general agreement with those reported previously for endogenous protein [51] and as found from Western blot data ($T_{1/2}$=40 min) (**Fig.14C**).

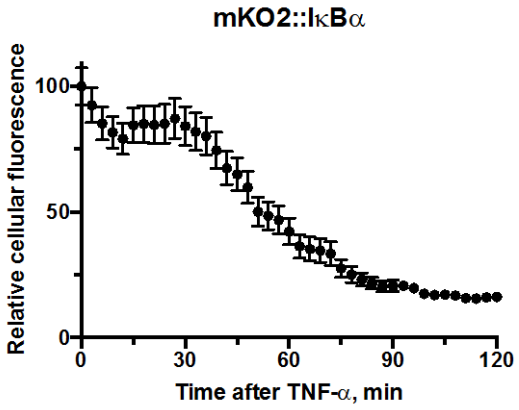


**Fig. 17. Degradation of mKO2::IκBα in response to TNFα stimulation**. Transfected HeLa cells were stimulated with 10 ng/mL TNFα and monitored for 2 h. Mean cellular fluorescence intensities were determined for fluorescent cells at each time point and plotted as a percentage of fluorescent values at t=0 min. Data shown as mean ±SD with at least 10 cells per experiment.

In transfected cells expressing mKO2::IκBα74-PEST(IκBαΔANK1-6), degradation reached 50% of initial cellular fluorescence in 48 min (**Fig. 18**).

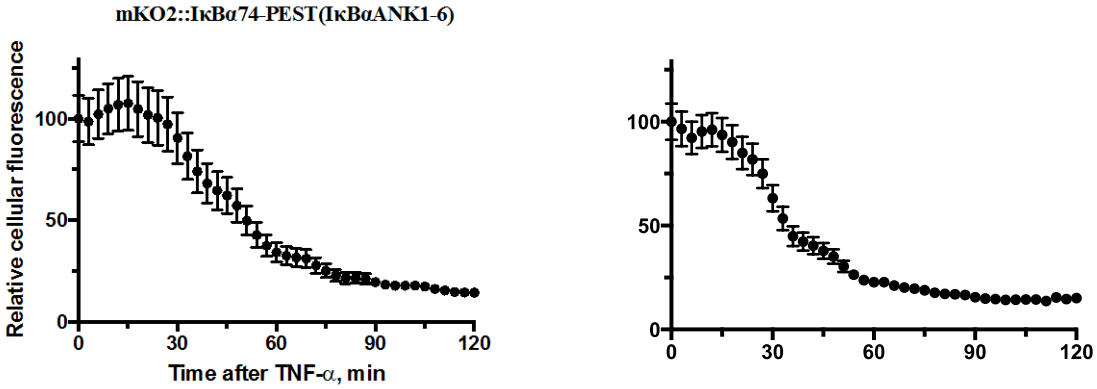


**Fig. 18. Degradation of mKO2::IκBα74-PEST(IκBαΔANK1-6) and mKO2::IκBα140-PEST(IκBαΔANK3-6) in response to TNFα stimulation.** Degradation of mKO2::IκBα74-PEST(IκBαΔANK1-6) (left) or mKO2::IκBα140-PEST(IκBαΔANK3-6) (right) proteins expressed in transfected HeLa cells was quantified and mean cellular fluorescence intensities were determined as described in Fig. 17. Results show mean values ±SD with at least 10 cells per experiment.

This was longer than the $T_{1/2}$ for mKO2::IκBα (see above). In contrast degradation rate of mKO2::IκBα140-PEST(IκBαΔANK3-6) ($T_{1/2}$ = 30 min) was shorter than mKO2::IκBα74-PEST(IκBαΔANK1-6) and mKO2::IκBα (**Fig. 18**). The rate of mKO2::IκBα therefore more closely resembled the rate of endogenous IκBα degradation [14, 51, 52].

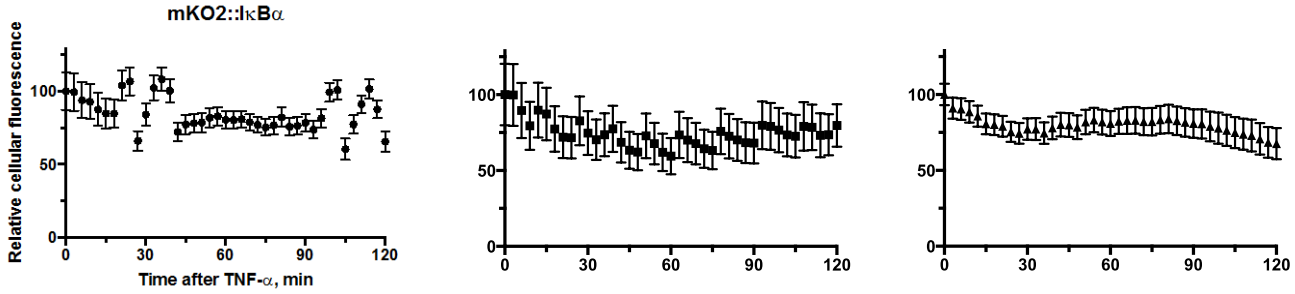


**Fig. 19. Degradation of fusion proteins in response to TNFα in presence of lactacystin.** Mean cellular fluorescence intensities were determined for fluorescent cells at each time point and plotted as a percentage of fluorescent values at t=0 min. Cells were treated with 25 μM lactacystin 24 h prior to stimulation with 10 ng/mL TNFα at t=0 min. Data shown as mean ±SD with at least 10 cells per experiment.

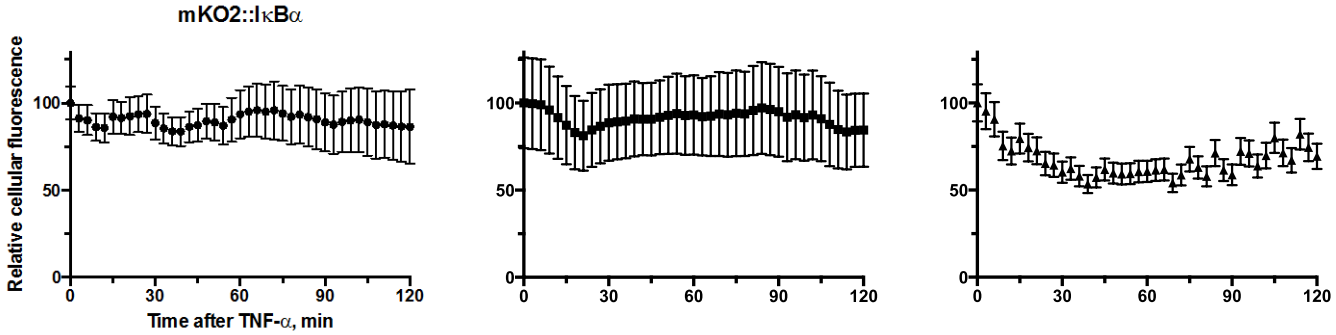


**Fig. 20. Degradation of fusion proteins in response to TNFα in presence of MG132.** Mean cellular fluorescence intensities were determined for fluorescent cells at each time point and plotted as a percentage of fluorescent values at t=0 min. Cells were treated with 50 μM MG132 24 h prior to stimulation with 10 ng/mL TNFα at t=0 min. Data shown as mean ±SD with at least 10 cells per experiment.

I used the concentrations of lactacystin and MG132, which were previously shown to significantly inhibit TNFα-induced proteasomal degradation of IκBα [49, 50]. The degradation of fusion proteins following TNFα stimulation was inhibited by pretreatment with 25 μM lactacystin (**Fig. 19**) and 50 μM MG132 (**Fig. 20**). The inhibitory effect of

lactacystin and MG132 supports the hypothesis that the observed fluorescence decrease is due to TNFα-induced degradation of fusion proteins via ubiquitin-proteasomal pathway.

Furthermore, I tested the effect of proteasomal inhibitors at lower doses and monitored the degradation for 2 hours using transfected cells expressing mKO2::IκBα140-PEST(IκBαΔANK3-6), to evaluate sensitivity and applicability of this platform to screen agents targeting proteasomal pathway. Lactacystin at 10 μM inhibited degradation for 2 hours, however inhibitory effect was less than that of 25 μM dose. One micromole dose of lactacystin did not effectively inhibit the degradation compared to higher doses (**Fig. 21**). This suggests that this platform could be useful for dose-dependent evaluation of inhibitors targeting NF-κB pathway as a first-pass screening tool.

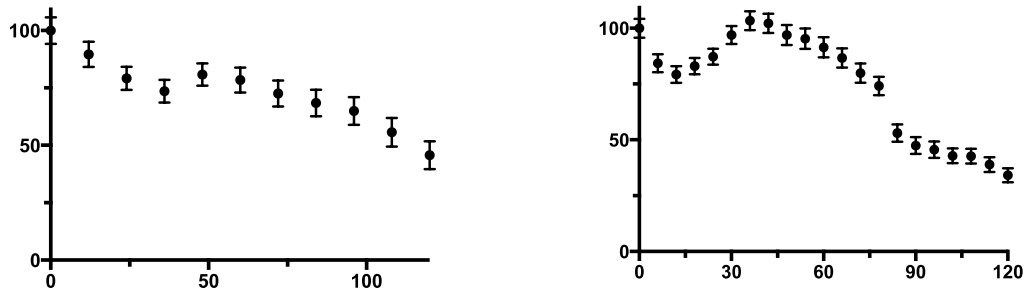


**Fig. 21. Degradation of fusion proteins in response to TNFα in presence of lactacystin.** Mean cellular fluorescence intensities were determined for fluorescent cells at each time point and plotted as a percentage of fluorescent values at t=0 min. Cells were treated either with 10 μM lactacystin (left) or 1 μM lactacystin (right) 24 h prior to stimulation with 10 ng/mL TNFα at t=0 min. Data shown as mean ±SD with at least 10 cells per experiment.

### II.3 Conclusion

Real-time confocal microscopy and western blot analysis showed that, like endogenous IκBα, fusion-proteins expressed in HeLa cells degraded after TNFα stimulation. Decrease of fluorescence intensity was observed at approximately 5-7 minutes post-stimulation with TNFα. In this *in vitro* setting, degradation dynamics of recombinant probes were comparable to those observed with endogenous IκBα. No decrease in fluorescence was observed in the cells transfected with mKO2 alone, suggesting that degradation of fluorescent proteins occurs only if fused to IκBα. Fusion

proteins lacking the PEST motif exhibited no stimuli-induced degradation, as monitored by time-lapse fluorescence imaging. From confocal microscopy data obtained for fusion proteins with mutations at PEST site, it is concluded that PEST sequence is essential in signal-induced degradation of IκBα and functions independently from ANK repeats. Proteasome inhibitors such as lactacystin and MG132 blocked the decay of fluorescence in all PEST-containing degradable probes, suggesting that degradation of fusion proteins in stimulated cells occurs via proteasomal system. The degradation rate of mKO2::IκBα74-PEST(IκBαΔANK1-6) was slower than mKO2::IκBα140-PEST(IκBαΔANK3-6) and mKO2::IκBα proteins, which in turn was similar to the half-life of native IκBα.

# Chapter III

# Structure-activity relationship of fusion proteins: an *in silico* analysis

## III.1 Materials and Methods

### III.1.1 Homology modeling

I used I-TASSER protein structure prediction algorithm based on multiple template assembly, which combines the methods of threading, *ab initio* modeling, homology modeling and structural refinement, to predict the structure of fusion proteins [53-55]. I-TASSER was ranked the No. 1 server for protein structure prediction in recent CASP7, CASP8 and CASP9 experiments [56, 57]. The FASTA sequence of mKO2::IκBα protein (MVSVIKPEMKMRYYMDGSVNGHEFTIEGEGTGRPYEGHQEMTLRVTMAEGGP MPFAFDLVSHVFCYGHRVFTKYPEEIPDYFKQAFPEGLSWERSLEFEDGGSASVS AHISLRGNTFYHKSKFTGVNFPADGPIMQNQSVDWEPSTEKITASDGVLKGDVT MYLKLEGGGNHKCQMKTTYKAAKEILEMPGDHYIGHRLVRKTEGNITEQVEDA VAHWYQPLEVDGIDKLDGGGGSGGGGSGGGGSIEFFQAAERPQEWAMEGPRDG LKKERLLDDRHDSGLDSMKDEEYEQMVKELQEIRLEPQEVPRGSEPWKQQLTED GDSFLHLAIIHEEKALTMEVIRQVKGDLAFLNFQNNLQQTPLHLAVITNQPEIAEA LLGAGCDPELRDFRGNTPLHLACEQGCLASVGVLTQSCTTPHLHSILKATNYNG HTCLHLASIHGYLGIVELLVSLGADVNAQEPCNGRTALHLAVDLQNPDLVSLLL KCGADVNRVTYQGYSPYQLTWGRPSTRIQQQLGQLTLENLQMLPESEDEESYDT ESEFTEFTEDELPYDDCVFGGQRLTL*) was first threaded through the PDB database [58] to reveal appropriate local fragments, which were used for further structural assembly. 3D models are built based on multiple-threading alignments used by LOMETS algorithm and iterative TASSER assembly simulations. The continuous fragments with more than 5 residues are then extracted from the LOMETS alignments and used to reassemble the structure by replica-exchange Monte Carlo simulations [59]. The simulation trajectories are then clustered by SPICKER algorithm [60] and are used as the starting state of the second round I-TASSER assembly simulation. The final threading templates used by I-TASSER to predict mKO2::IκBα protein were the crystal structures of d34 region of human ankyrin-r and linker (PDB: 1N11A), TGP, an extremely thermostable green fluorescent protein (PDB: 4TZA), red fluorescent protein mKeima (PDB: 3IR8), AnkB 24 ankyrin repeats in complex with AnkR autoinhibition segment (PDB: 4RLV), monomeric Kusabira-Orange (mKO) (PDB: 2ZMU), Myo3b-ARB2 in complex with Espin1-AR (PDB: 5ET0). Finally, the structures of the lowest energy were

selected, which were then refined by molecular dynamics, with the purpose of removing steric clashes, minimizing violations of spatial restraints and optimizing the hydrogen-bonding network. The same procedure was applied to predict the structure of mKO2::IκBα74-PEST(IκBαΔANK1-6). However, for mKO2::IκBα140-PEST(IκBαΔANK3-6), I-TASSER could not correctly fold the protein. In that case, the homology modeling was employed with the optimized structure of mKO2::IκBα as a template using the molecular modeling environment Maestro v. 10.6 (Schrödinger, LLC., NY). Model for mKO2::IκBα140-PEST(IκBαΔANK3-6) was independently constructed with logic for proper handling of the sequence insertions and deletions. Missing loops were built using *ab initio* protein prediction approach with Prime program [61, 62].

### III.1.2 Molecular dynamics

I conducted MD simulations for three proteins, mKO2::IκBα, mKO2::IκBα140-PEST(IκBαΔANK3-6) and mKO2::IκBα74-PEST(IκBαΔANK1-6) starting from the energy minimized structure in each case. All MD simulations were performed using Desmond package [63-65] with an OPLS3 force field [66]. The simulations were conducted in explicit solvent. The initial structure was inserted into an orthorhombic box. A simulation cell was constructed around the model with a 9 Å cutoff for Lennard-Jones forces and the direct space portion of electrostatic forces, which were calculated using the Particle Mesh Ewald method. The resulting system was solvated with transferable intermolecular potential three-point (TIP3P) water molecules [67]. The counter ions, $Na^+$ or $Cl^-$ were added to neutralize the system. NaCl (0.15M) solution was added to simulate the background salt and physiological conditions. The pKa values of the ionizable groups in the model were calculated and used to assign the protonation states based on pH 7.4 using PROPKA algorithm [68]. The entire system was energy minimized until the RMSD gradient values decreased below 0.01 kcal/mol/Å. The system was heated from 0 to 300 K for 100 ps. Following minimization and heating, 2 ns production simulation was conducted with a 1 fs time step at a pressure of 1 atm and a temperature of 300 K using Berendsen thermostat. The final snapshot at the end of the simulation was used as a reference to calculate the root mean square deviation (RMSD) for each amino acid during

the last 2 ns MD trajectory. The RMSD calculations obtained from the MD simulations for each case were conducted only after the protein had reached an equilibrium stable state.

### III.1.3 Assessment of the models

The quality of protein geometry was checked by using ProQ [69]. Protein superposition server SuperPose Version 1.0 was used to generate the RMSD statistics [70]. Molecular electrostatics involved in the structural analysis was performed using PyMol and Maestro programs.

### III.1.4 Protein-protein docking and binding site prediction

I used pairwise docking for mKO2::IκBα–p65/p50, mKO2::IκBα74-PEST(IκBαΔANK1-6)–p65/p50 and mKO2::IκBα140-PEST(IκBαΔANK3-6)–p65/p50 complexes. The structures of fusion proteins for docking were obtained from the final snapshots of MD simulation. Prior to docking, only the PDB coordinates of p65/p50 heterodimer (PDB ID: 1IKN) were preprocessed for energy minimization using the OPLS3 force field. Molecular docking was performed with Fast Fourier Transform (FFT) correlation approach using the protein-protein docking software PIPER [71, 72] that evaluates the energies of billions of docked conformations on a grid. The final docked complexes were subjected to energy minimization in three steps. Partial charges were assigned to the protein after adding each of the hydrogen atoms using the OPLS3 force field. In the first step, constraints were applied to the heavy atoms, by allowing the mobility of all hydrogen atoms. In the second energy minimization step, only the backbone chain was constrained, whereas the side chains were allowed to move. In the third energy minimization round, only the Cα atoms were constrained, and all other atoms were allowed to move. All of the above energy minimizations were conducted using both the steepest descent and conjugate gradient protocols. The buried surface interaction areas of the complex models were calculated using the Maestro program (protein-protein interface analysis).

### III.2 Results and Discussion

#### III.2.1 Comparative modeling of fusion proteins

First, homology modeling of the structure of mKO2::IκBα and mKO2::IκBα74-PEST(IκBαΔANK1-6) using I-TASSER was performed. I-TASSER (Iterative Threading ASSEmbly Refinement) is a computational method that has been extensively used in accurately modeling protein structures [53-56]. I-TASSER uses a combinatorial approach, employing three conventional methods for structure modeling: homology (comparative), threading, and *ab initio* modeling [53]. For the submitted sequences, five models of each mKO2::IκBα and mKO2::IκBα74-PEST(IκBαΔANK1-6) were generated with C-scores ranging from −0.95 to −3.04 and -0.06 to -3.31 respectively. The C-score is a confidence score and in the range of [−5, 2], with higher scores representing higher confidence in the model and vice-versa [55].

**A**

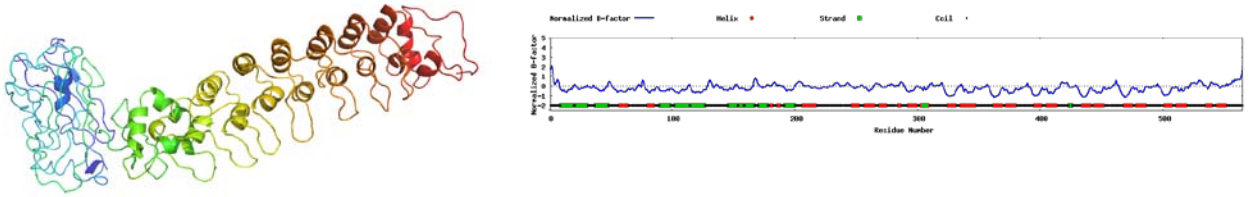

**B**

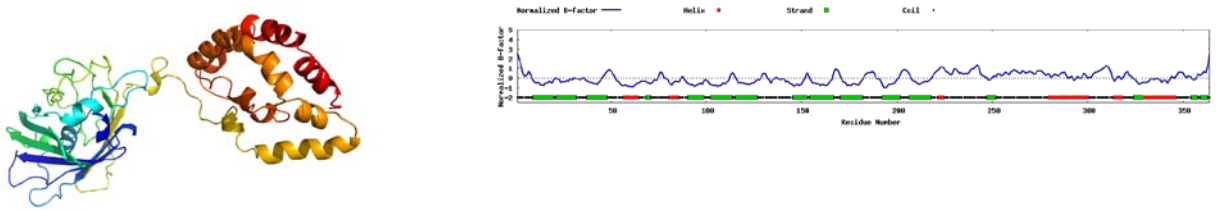

**C**

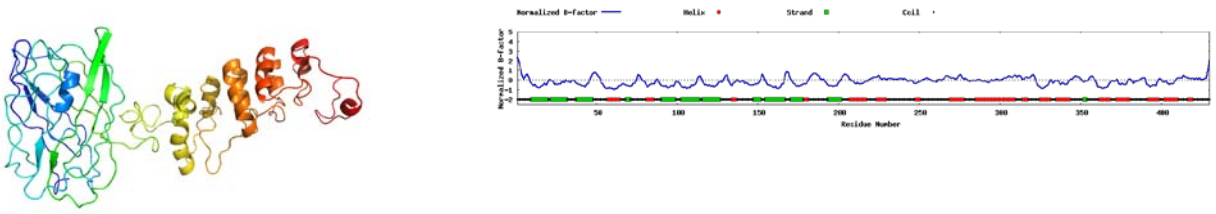

**Fig. 22. Tertiary structures of fusion proteins.** Structures of the resulting homology models of (A) mKO2::IκBα, (B) mKO2::IκBα74-PEST(IκBαΔANK1-6) and (C) mKO2::IκBα140-PEST(IκBαΔANK3-6) with predicted normalized B-factor profiles of the targets created with I-TASSER and rendered with PyMol.

The C-score value being lower than -1.5 likely indicates a lack of an appropriate template within the I-TASSER library. Model 1 of both mKO2::IκBα (C-score = -0.95, **Fig. 22A**) and mKO2::IκBα74-PEST(IκBαΔANK1-6) (C-score = -0.06, **Fig. 22B**) were used for all further analyses. In the case of mKO2::IκBα140-PEST(IκBαΔANK3-6) (**Fig. 22C**) MD optimized mKO2::IκBα structure was used as a template for *ab initio* protein modeling. The sequence alignment of mKO2::IκBα140-PEST(IκBαΔANK3-6) was carried out and manually adjusted to ensure alignment of important functional residues. Missing residues and loops were *ab initio* modeled using PRIME program. ANK repeats of the constructed models of fusion proteins depicted two anti-parallel α-helices, followed by a loop of variable length at a right angle. Each repeat began and ended with short β-hairpin turns that protruded away from α -helix. This non-globular fold was stabilized through intra- and inter-repeat hydrophobic interactions. Normalized B-factor values for fusion proteins predicted using a combination of both template-based assignment and profile-based prediction are shown in **Fig. 22**. Residues with positive B-factor values are less stable in experimental structures whereas negative values show more stable fragments. Residues located in loops or C- and N-terminal regions tend to have higher predicted B-factor values, as they are usually less stable compared with residues located at helices or strands.

**Table 2. Top 10 threading structures used for homology sequencing.**

| | **mKO2::IκBα** | | | | | **mKO2::IκBα74-PEST(IκBαΔANK1-6)** | | | | |
|---|---|---|---|---|---|---|---|---|---|---|
| **Rank** | **PDB Hit** | **Iden1** | **Iden2** | **Cov** | **Norm. Z-score** | **PDB Hit** | **Iden1** | **Iden2** | **Cov** | **Norm. Z-score** |
| 1 | 1N11A | 0.20 | 0.19 | 0.64 | 3.49 | 2ZMUA | 0.95 | 0.56 | 0.59 | 2.34 |
| 2 | 4TZAC | 0.53 | 0.21 | 0.37 | 1.78 | 4JRBA | 0.16 | 0.20 | 0.96 | 3.31 |
| 3 | 1N11A | 0.20 | 0.19 | 0.66 | 3.33 | 2ZMUA | 0.96 | 0.56 | 0.59 | 3.88 |
| 4 | 3IR8A | 0.51 | 0.19 | 0.37 | 1.83 | 3MGFA | 0.95 | 0.56 | 0.58 | 3.24 |
| 5 | 4RLVA | 0.19 | 0.21 | 0.94 | 3.56 | 3CGLA | 0.46 | 0.30 | 0.60 | 1.98 |
| 6 | 2ZMUA | 0.96 | 0.36 | 0.36 | 5.31 | 2C9IA | 0.45 | 0.29 | 0.61 | 1.44 |
| 7 | 4RLVA | 0.14 | 0.21 | 0.90 | 12.40 | 2ZMUA | 0.95 | 0.56 | 0.59 | 3.31 |
| 8 | 4RLVA | 0.17 | 0.21 | 0.90 | 4.64 | 4TZAC | 0.53 | 0.32 | 0.58 | 2.22 |
| 9 | 5ET0A | 0.17 | 0.15 | 0.57 | 2.11 | 2ZMUA | 0.96 | 0.56 | 0.59 | 6.58 |
| 10 | 4RLVA | 0.19 | 0.21 | 0.84 | 3.24 | 2ZO6A | 0.62 | 0.37 | 0.59 | 4.81 |

Rank of templates represents the top ten threading templates used by I-TASSER. Iden1 is the percentage sequence identity of the templates in the threading aligned region with the query sequence. Iden2 is the percentage sequence identity of the whole template chains with query sequence. Cov represents the coverage of the threading alignment and is equal to the number of aligned residues divided by the length of query protein. Norm. Z-score is the normalized Z-score of the threading alignments. Alignment with a Normalized Z-score >1 mean a good alignment and vice versa.

The structures of fusion proteins were used to search for proteins with regions of structural homology within the PDB database (**Table 2**). This assessment was carried out using the TM-align program [73]. TM-align detects the structural and functional analogs from the PDB library by the global structural alignment algorithm. Although the overall goal of the TM-align was to identify structural homologs, this server was utilized in order to give a deeper insight into the relationship between the modeled structure of fusion proteins and other proteins of known structure. The TM-align search indicated that the 10 proteins share structural similarity to the fusion proteins (**Table 3**) including monomeric Kusabira Orange and ankyrin containing proteins. Estimated RMSDs for mKO2::IκBα, mKO2::IκBα74-PEST(IκBαΔANK1-6) and mKO2::IκBα140-PEST(IκBαΔANK3-6) were found to be 9.8±4.6Å, 6.7±4.0Å and 9.3±4.6Å respectively.

**Table 3. Proteins structurally close to the target mKO2::IκBα in the PDB.**

| Rank | PDB Hit | TM-score | RMSD[a] | Iden[b] | Cov |
|---|---|---|---|---|---|
| 1 | 4RLVA | 0.853 | 3.34 | 0.145 | 0.945 |
| 2 | 1N11A | 0.615 | 2.12 | 0.191 | 0.650 |
| 3 | 3L5Q6 | 0.548 | 6.53 | 0.043 | 0.811 |
| 4 | 3JAVA | 0.519 | 6.89 | 0.070 | 0.782 |
| 5 | 4UVKA | 0.509 | 7.09 | 0.045 | 0.800 |
| 6 | 1B3UA | 0.498 | 6.18 | 0.047 | 0.710 |
| 7 | 2XWUB | 0.483 | 6.13 | 0.055 | 0.687 |
| 8 | 4PJUA | 0.474 | 6.96 | 0.043 | 0.731 |
| 9 | 3ICQU | 0.463 | 6.64 | 0.051 | 0.683 |
| 10 | 4IFQA | 0.460 | 6.52 | 0.021 | 0.669 |

TM-score, ranking of proteins of the structural alignment between the mKO2::IκBα and known structures in the PDB library. [a)] RMSD between residues that are structurally aligned by TM-align. [b)] Iden is the percentage sequence identity in the structurally aligned region. Cov represents the coverage of the alignment by TM-align and is equal to the number of structurally aligned residues divided by length of the query protein.

### III.2.2 Structure refinement and stability evaluation

Predicted structures of fusion proteins were subjected to MD simulation in order to assess the stability of the models. **Fig. 23** shows the root mean square deviation (RMSD) and root mean square fluctuation (RMSF) plots for the protein Cα-atoms and other heavy atoms with reference to the initial structure as a function of time. The plot shows that the equilibrium state was reached after 0.5 ns of simulation and was kept constant until the

end of the dynamics. Changes of RMSF peaks indicate areas of the protein that fluctuate the most during the simulation. Tails (N- and C-terminal) as wells as GS-linker region fluctuate more than any other parts of the protein.

**A**

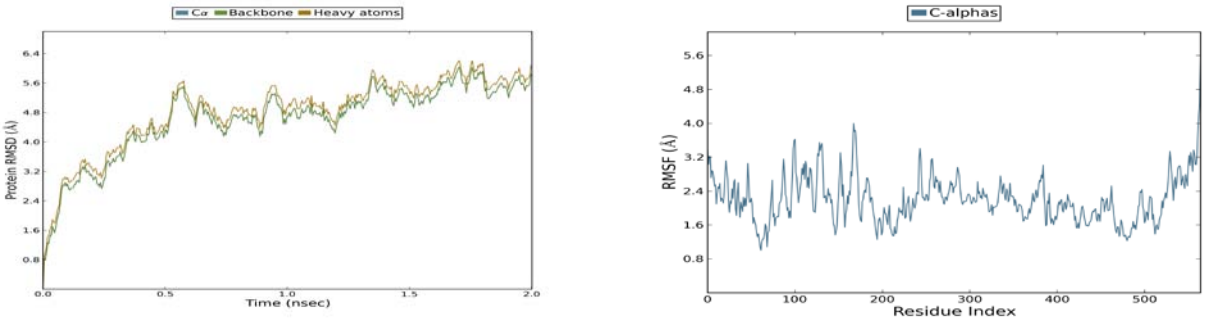


**B**

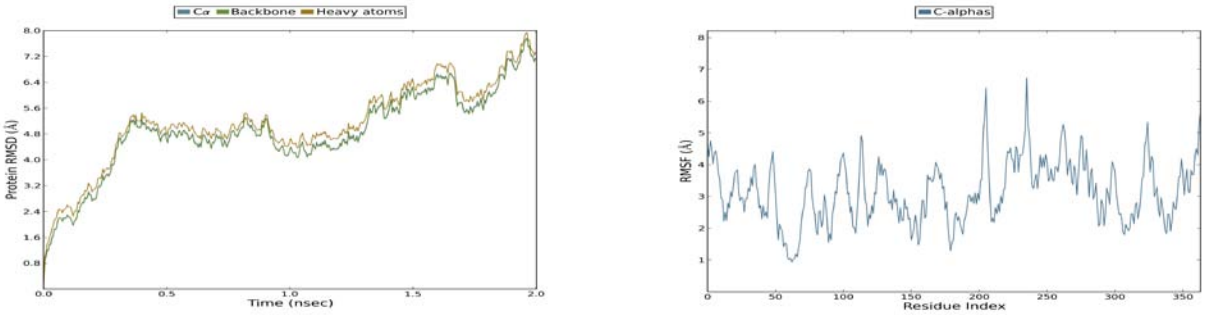


**C**

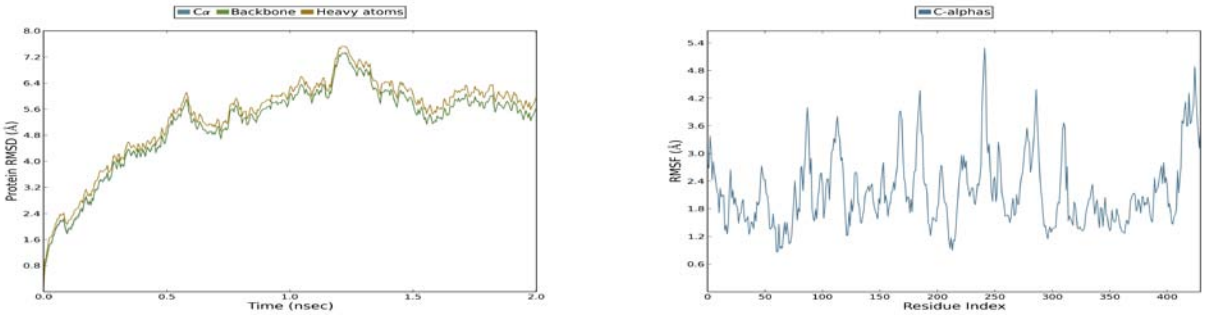


**Fig. 23. Molecular dynamics trajectory-based analysis of the model refinement.** RMSD and RMSF of Cα of (A) mKO2::IκBα (B) mKO2::IκBα140-PEST(IκBαΔANK3-6) and (C) mKO2::IκBα74-PEST(IκBαΔANK1-6) with respect to their initial structure show the stable nature of the model after an initial equilibration time.

Secondary structure elements like alpha helices and beta strands are more rigid than the unstructured parts of the protein, and thus mKO2::IκBα with 6 ANKs fluctuates less than mKO2::IκBα140-PEST(IκBαΔANK3-6) (2 ANKs) and mKO2::IκBα74-PEST(IκBα

ΔANK1-6) (no ANKs). Structural rearrangements of superimposed initial structure with the final refined structure in each case are shown in **Table 4**.

**Table 4. RMSD (Å) values between the initial and MD refined structures compared using SuperPose.**

| | Alpha Carbons | Backbone | Heavy atoms | All atoms |
|---|---|---|---|---|
| **mKO2::IκBα** | 3.04 | 3.07 | 3.33 | 3.45 |
| **mKO2::IκBα140PEST (IκBαΔANK3-6)** | 3.64 | 3.64 | 3.73 | 3.78 |
| **mKO2::IκBα74-PEST (IκBα ΔANK1-6)** | 1.34 | 1.37 | 1.72 | 2.00 |

Evaluation of the stereochemical quality of the model showed that only a few residues are in disallowed regions in the Ramachandran plot and most of them correspond to the structurally non-conserved regions (**Fig. 24**). These models show an improved energy profile compared with the initial models.

**mKO2::IκBα** **mKO2::IκBα140PEST (IκBαΔANK3-6)** **mKO2::IκBα74-PEST (IκBα ΔANK1-6)**

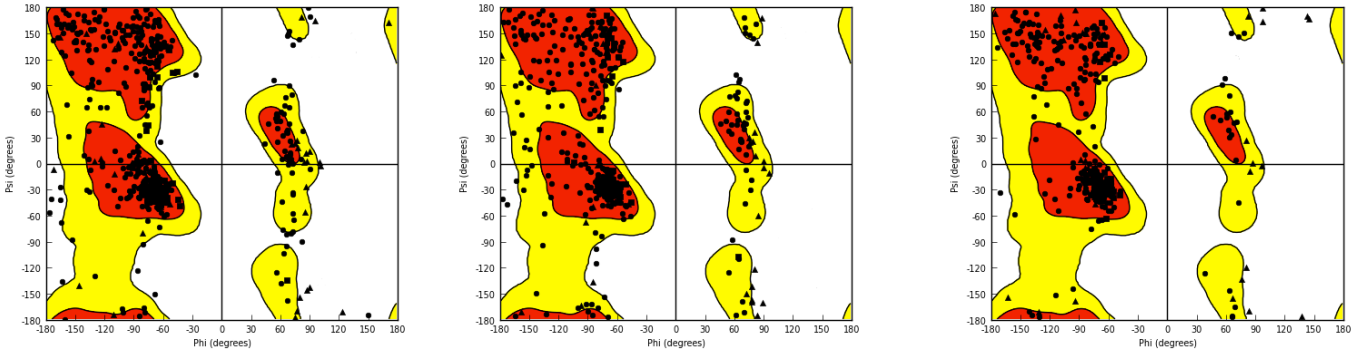


**Fig. 24. Ramachandran plot for the minimized structures of fusion proteins.** Glycine is plotted as triangles, proline is plotted as squares, all other residues are plotted as circles.The orange regions are the "favored" regions, the yellow regions are the "allowed" regions, and the white regions are the "disallowed" regions.

**Table 5. Model evaluation.**

| | ProQ LGscore | ProQ MaxSub |
|---|---|---|
| mKO2::IκBα | 3.843 | 0.631 |
| mKO2::IκBα140-PEST(IκBαΔANK3-6) | 3.732 | 0.588 |
| mKO2::IκBα74-PEST(IκBα ΔANK1-6) | 2.875 | 0.307 |

Note: LGscore is -log of a P-value and MaxSub ranges from 0-1, were 0 is insignificant and 1 very significant. LGscore >1.5 fairly good model; >2.5 very good model; >4 extremely good model. MaxSub >0.1 fairly good model; >0.5 very good model; >0.8 extremely good model.

I took the final snapshots of mKO2::IκBα, mKO2::IκBα74-PEST(IκBαΔANK1-6) and mKO2::IκBα140-PEST(IκBαΔANK3-6) and subjected them to energy minimization following the model evaluation, which involved analysis of geometry, stereochemistry and energy distribution of the optimized models. The evaluation listed in **Table 5** indicated high quality for all of the models in terms of overall packing. These models were subsequently used for protein-protein docking studies.

### III.2.3 Pairwise docking of mKO2-IκBα–NF-κB complex

The structural interactions between IκBα and p65/p50 have been described previously [17]. I utilized PIPER, a protein-protein docking program that uses rigid body global search based on the Fast Fourier Transform (FFT) correlation approach to assess the interaction of protein molecules, to identify the likely binding sites of the p65/p50 heterodimer interfaces with fusion-proteins, as well as to evaluate the effect of the mutations (see Chapter II) in binding and degradation process. The structure of p65/p50 heterodimer was extracted from the PDB database (1IKN) [17]. The procedure of protein-protein docking is highly computationally oriented. The reliability of the docking results strongly depends on the quality of the docking methods. Each docking returned the 100 most probable models. The optimal docking solution for each complex was selected from the 100 candidates based on the following criteria: models that do not exist in the intersection of the two resulting sets were excluded; include only those shared models in which the binding region is supported by the literature data [17, 18]. In addition to the available literature information, a comparative study clearly demonstrated that full-length

mKO2::IκBα has association with p65 NLS, located near the dimerization domain (**Fig. 25**).

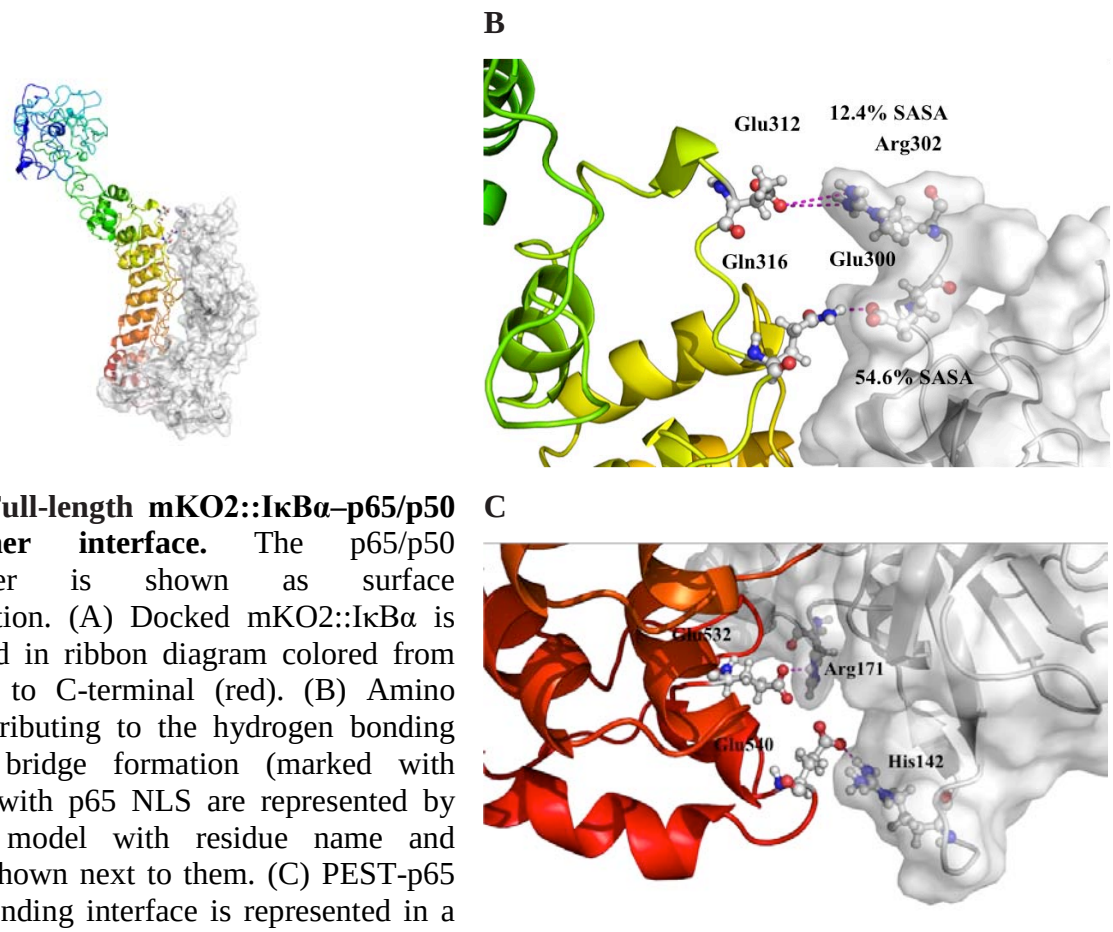


**Fig. 25. Full-length mKO2::IκBα–p65/p50 heterodimer interface.** The p65/p50 heterodimer is shown as surface representation. (A) Docked mKO2::IκBα is represented in ribbon diagram colored from N- (blue) to C-terminal (red). (B) Amino acids contributing to the hydrogen bonding and salt bridge formation (marked with magenta) with p65 NLS are represented by ball-stick model with residue name and numbers shown next to them. (C) PEST-p65 RHD-N binding interface is represented in a similar manner as in (B).

Anionic carboxylate of Glu312 of ANK1 forms salt bridge with cationic guanidinium of Arg302 of nuclear localization signal. This interaction buries 12.4% of solvent accessible surface area (SASA). Gln316 of ANK2 forms H-bond with Glu300 of NLS. This interaction buries 54.6% of SASA. In addition, Trp314, Gln344, Phe351 of ANK1 are projected towards the NLS of p65. Thus ANK1 and ANK2 mask NLS stabilizing NF-κB in cytoplasm and this is in agreement with previously solved cytoplasmic IkBα protein [17, 18]. Moreover, anionic carboxylate of Glu532 of PEST forms salt bridge with cationic guanidinium of Arg171 of p65 and buries 46.6% of SASA. Glu540 of PEST forms H-bond with His142 of RHD of p65 and buries 69.6% of SASA (**Fig. 25**). Interactions between mKO2::IκBα protein and NF-κB in total bury 402 Å $^2$ of solvent accessible surface area, with 16 H-bonds along with long-range salt bridges. It was

previously reported that signal-induced degradation of IκBα via the ubiquitin-proteasomal pathway requires phosphorylation on N-terminal residues serine 32 and 36 following the ubiquitination on Lys21 and 22 of IκBα [43, 44]. Flexible (GGGGS)3x linker keeps the mKO2 in distance from the phosphorylation and ubiquitination domains of IκBα providing the enough solvent accessibility to these residues for the degradation enzymes. SASA for Ser32, Ser36, Lys21 and Lys22 were calculated to be 31, 43, 58, 140 $Å^2$ respectively (**Fig. 26**).

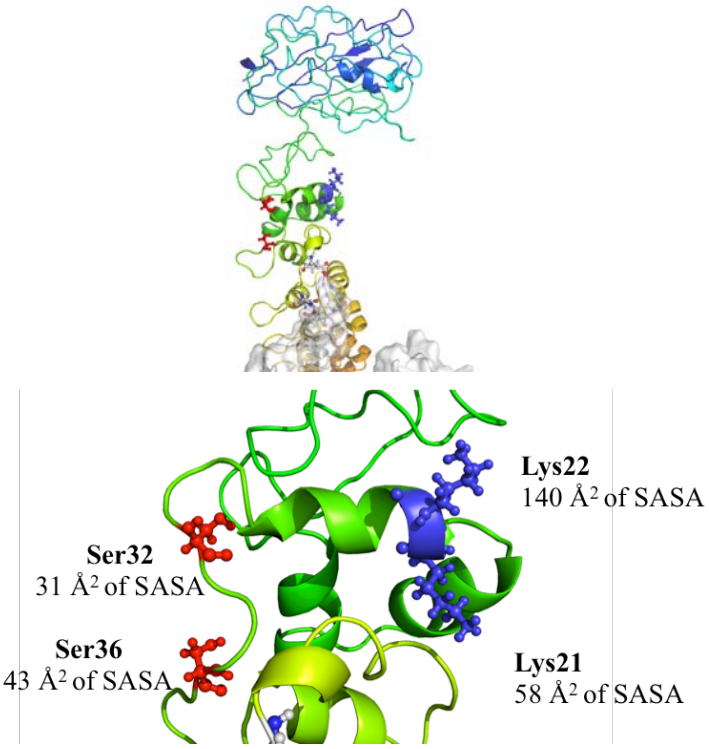


**Fig. 26. mKO2::IκBα–p65/p50 heterodimer interface.** Docking studies predict that the GS-linker keeps the mKO2 in distance from the phosphorylation and ubiquitination domains providing solvent accessibility to Ser32, Ser36 (red) and Lys21, Lys22 (blue). Backbone is represented as described in Fig. 25.

mKO2::IκBα140-PEST(IκBαΔANK3-6) interacts with NF-κB in a similar mode to the full-length fusion protein. However, ANK1 and ANK2 were displaced unmasking NLS (**Fig. 27**). Solvent accessibility of ubiquitination domains Lys21 (SASA 59 $Å^2$) and Lys22 (SASA 139 $Å^2$) and phosphorylation domain Ser36 (SASA 40 $Å^2$) were similar to residues in full-length fusion protein. However, this displacement resulted in solvent accessibility of phosphorylation site Ser32 increased from 31 to 55 $Å^2$, suggesting the reason for faster degradation compared to mKO2::IκBα.

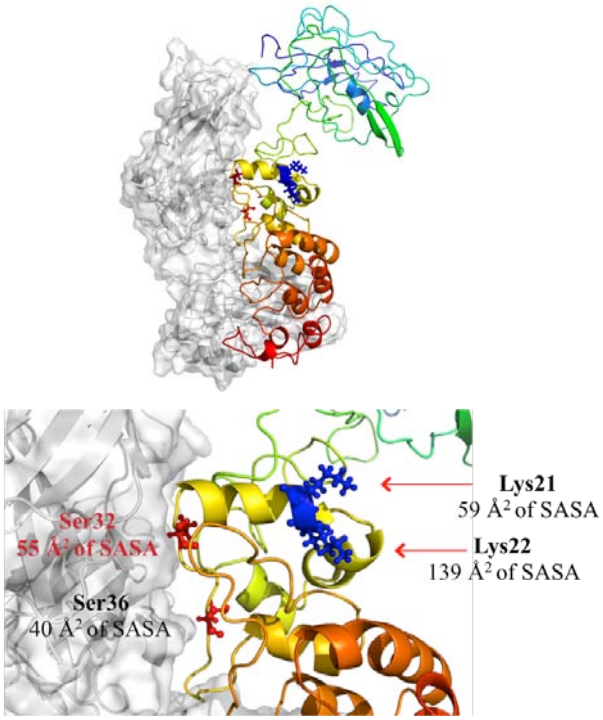


**Fig. 27. mKO2::IκBα140-PEST(IκBαΔANK3-6) – p65/p50 heterodimer interface.** Displacement of ANK1 and ANK2 resulted in elevated SASA for Ser32 (red) from 31 to 55 Å$^2$.

mKO2::IκBα74-PEST(IκBαΔANK1-6) does not contain ANK repeats. It contains only C-terminal PEST domain and N-terminal of IκBα, which was fused to mKO2. These domains of mKO2::IκBα74-PEST(IκBαΔANK1-6) interacts with RHD-N of p65 as in other constructs. This association resulted in decrease of SASA from 58 and 140 to 16 and 40 Å$^2$ for both ubiquitination residues Lys21 and Lys22 respectively, suggesting the possible reason for slower degradation (**Fig. 28**) compared to fusion proteins with longer IκBα. Computational structure-activity studies show consistency between fusion protein structures, their interaction with NF-κB subunits and degradation kinetics.

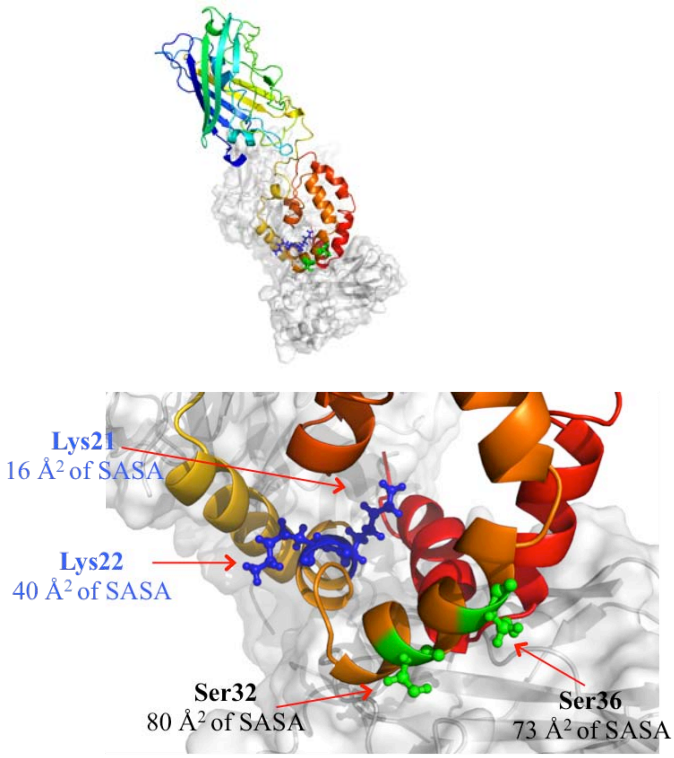


**Fig. 28. mKO2::IκBα74-PEST(IκBαΔANK1-6) – p65/50 interface.** C-terminal of mKO2::IκBα74-PEST(IκBαΔANK1-6) interacts with RHD-N of p65. SASA for Lys21 (58 $Å^2$) and Lys22 (140 $Å^2$) (blue) decreased to 16 and 40 $Å^2$ respectively.

### III.3 Conclusion

The three-dimensional structures of mKO2::IκBα, mKO2::IκBα74-PEST(IκBαΔANK1-6) and mKO2::IκBα140-PEST(IκBαΔANK3-6) were modeled using comparative (homology) modeling approach. Subsequently, molecular dynamic simulations of these proteins in the presence of explicit water were performed to optimize the models and assess the stability. The confidence of the models was quantified based on the significance of threading template alignments and the convergence parameters of the structure assembly simulations. Models of mKO2::IκBα (C-score=-0.95, RMSD=9.8±4.6Å), mKO2::IκBα74-PEST(IκBαΔANK1-6) (C-score=-0.06, RMSD=6.7±4.0Å) and mKO2::IκBα140-PEST(IκBαΔANK3-6) (C-score=-1.03, RMSD=9.3±4.6Å) were of correct global topology. ANK repeats of the designed models were described as two anti-parallel α-helices, followed by a loop at nearly right angle stabilized by the hydrophobic interactions within the repeats. In all constructs, GS-linker

allowed the mKO2 to keep distance from functional domains and N-terminal region of IκBα to be accessible for both phosphorylation and ubiquitination. Furthermore, the refined models by molecular dynamics were used for multiple protein-protein docking studies for the identification of their complexes with p65/p50 NF-κB subunits in order to study the effect of fusion construct to the stability of the complex as well as effect of mutations in binding and degradation processes. Fusion proteins did not create a single continuous buried surface contact with NF-κB but rather interacted through several independent smaller patches. mKO2::IκBα protein bound to NF-κB in a similar mode as IκBα by masking NLS segment of p65. Displacement of mKO2::IκBα140-PEST(IκBαΔANK3-6) resulted in increased solvent accessibility for phosphorylation domain Ser32 that resulted in faster degradation. Solvent accessibility of both ubiquitination residues Lys21 and Lys22 of mKO2::IκBα74-PEST(IκBαΔANK1-6) decreased resulting in slower degradation.

## Summary

Novel fusion proteins composed of fluorescent protein mKO2 and human IκBα or its fragments were developed to evaluate dynamics of stimulus-triggered degradation of IκBα in living cells. Real-time confocal microscopy analysis showed that fusion-proteins expressed in HeLa cells degraded after TNFα stimulation. The half-life of degradation of mKO2::IκBα74-PEST(IκBαΔANK1-6) was smaller than mKO2::IκBα140-PEST(IκBαΔANK3-6) and mKO2::IκBα proteins, which in turn was similar to the native IκBα. Mutation studies demonstrated that PEST sequence is essential in signal-induced degradation of IκBα independently from ANK repeats.

Selective proteasome inhibitors blocked the decay of fluorescence in concentration dependent manner, suggesting that stimuli-induced degradation of fusion proteins occurs via proteasomal system. Kinetics of degradation of these proteins obtained by real-time monitoring in the presence or absence of proteasome inhibitors upon the pro-inflammatory stimuli provided a reliable platform for the first-pass screening and evaluation of new drugs targeting the NF-κB pathway.

Molecular-modeling approach was used to obtain structural models and reveal the potential sites of interaction between fusion proteins and NF-κB as well as the effect of mutations in binding and degradation processes. The mKO2::IκBα bound to NF-κB similarly as native IκBα masking nuclear localization domain. In all proteins GS-linker kept mKO2 in a distance from phosphorylation and ubiquitination sites of IκBα to provide enough accessibility for the enzymes. Different binding schemes of partially modified IκBα fusion proteins with NF-κB altered surface accessible solvent area for phosphorylation and ubiquitination residues resulting in changed kinetics of degradation, which was consistent with microscopy data. The technique that has been described here could provide a range of possible applications, such as the analysis of the dynamics and biochemical characteristics of IκBα degradation as well as for screening of potential proteasomal inhibitors.

## Acknowledgments

I would like to express my sincere gratitude to my advisor Professor Mitsuru Hashida for the continuous support, for his patience and motivation throughout this study. I could not have imagined having a better advisor and mentor for my research.

I would like to thank Professor Fumioshi Yamashita and Dr. Yuriko Higuchi for their consistent support, insightful comments and critiques, which incented me to widen my research from various perspectives. Your discussion, ideas, and feedback have been absolutely invaluable.

My sincere appreciation also goes to Professor Yoshinobu Takakura and all other members of thesis committee for their guidance through this process.

I'd like to thank my fellow graduate students, and administration staff of our department and graduate school especially Ms. Takako Tatsukawa. I am very grateful to all of you.

I would especially like to thank my amazing family for the love, support, and constant encouragement I have gotten over the years. In particular, I would like to thank my parents, my sister, my cousins, my aunt and my grandparents. Especially, I would like to thank my grandfather, Professor Shirmammad Huseynov for always being an example of a great scientist for me, who encouraged me to get doctoral degree in the first place.

I want to thank my dear husband for his continued support and understanding my persistence in the graduate career and making completion of this thesis possible.

The last word goes for Sara, our baby girl, who has been the light of our life for the last one year and who has given me the extra strength and motivation to get things done. This thesis is dedicated to her and my grandfather.

## References


1. Vincent Bours, Mohamed Bentires-Alj, Anne-Cécile Hellin, Patrick Viatour, Pierre Robe, Sylvie Delhalle, Valérie Benoit, Marie-Paule Merville. Nuclear factor-κB, cancer, and apoptosis. *Biochem. Pharmacol.* 2000; 60:1085–1089.
2. Michael Karin, Anning Lin. NF- κB at the crossroads of life and death. *Nature Immunology* 2002; 3:221-227.
3. Baeuerle PA, Henkel T. Function and activation of NF-kappa B in the immune system. *Annu. Rev. Immunol*. 1994;12:141-79.
4. Sen R, Baltimore D. Inducibility of kappa immunoglobulin enhancer-binding protein Nf-kappa B by a posttranslational mechanism. *Cell.* 1986; 26:47(6):921-8.
5. Gilmore T.D. Introduction to NF-kappaB: players, pathways, perspectives. *Oncogene*. 2006; 30:25(51):6680-4.
6. Perkins N.D. Integrating cell-signalling pathways with NF-kappaB and IKK function. *Nat. Rev. Mol. Cell Biol*. 2007; 8(1):49-62.
7. Beg AA, Baldwin AS Jr. The I kappa B proteins: multifunctional regulators of Rel/NF-kappa B transcription factors. *Genes Dev*. 1993; 7(11):2064-70.
8. Baeuerle PA, Baltimore D. I kappa B: a specific inhibitor of the NF-kappa B transcription factor. *Science*. 1988; 28:242(4878):540-6.
9. Hayden MS, Ghosh S. Shared principles in NF-kappaB signaling. *Cell.* 2008; 132: 344-362.
10. Michel F, Soler-Lopez M, Petosa C, Cramer P, Siebenlist U. Crystal structure of the ankyrin repeat domain of Bcl-3: a unique member of the IkappaB protein family. *EMBO J*. 2001; 20: 6180–6190.
11. Perkins ND. Post-translational modifications regulating the activity and function of the nuclear factor kappa B pathway. *Oncogene.* 2006; 25:6717–6730.
12. Avraham Yaron, Ada Hatzubai, Matti Davis, Iris Lavon, Sharon Amit, Anthony M. Manning, Jens S. Andersen3, Matthias Mann3, Frank Mercurio2 & Yinon Ben-Neriah. Identification of the receptor component of the IkappaBalpha–ubiquitin ligase. *Nature* 1998; 396:590-594.

13. Coux O, Goldberg AL. Enzymes Catalyzing Ubiquitination and Proteolytic Processing of the p105 Precursor of Nuclear Factor κB1. *The Journal of Biological Chemistry*. 1998; 273:8820-8828.

14. Henkel T, Machleidt T, Alkalay I, Krönke M, Ben-Neriah Y, Baeuerle PA. Rapid proteolysis of I kappa B-alpha is necessary for activation of transcription factor NF-kappa B. *Nature*. 1993; 9:365(6442):182-5.

15. Kumar A, Takada Y, Boriek AM, Aggarwal BB. Nuclear factor-κB: its role in health and disease. *Journal of Molecular Medicine*. 2004; 82(7):434-448.

16. Chae Hyeong Lee, Yong-Tark Jeon, Su-Hyeong Kim, Yong-Sang Song. NF-κB as a potential molecular target for cancer therapy. *Biofactors*. 2007; 29:19-35.

17. T Huxford, D Huang, S Malek, G Ghosh. The Crystal Structure of the IκBα/NF-κB Complex Reveals Mechanisms of NF-κB Inactivation. *Cell*. 1998; 95:759-770.

18. MD Jacobs, SC Harrison. Structure of an IκBα/NF-κB Complex. *Cell*. 1998; 95:749-758.

19. Johanna Napetschnig and Hao Wu. Molecular Basis of NF-κB Signaling. *Annu. Rev. Biophys*. 2013; 42:443-468.

20. SC Sue, HJ Dyson. Interaction of the IκBα C-terminal PEST Sequence with NF-κB: Insights into the Inhibition of NF-κB DNA Binding by IκBα. *Journal of molecular biology*. 2009; 388:824-838

21. F Wan, MJ Lenardo. Specification of DNA binding activity of NF-κB proteins. *Cold Spring Harbor perspectives in Biology*. 2009.

22. CH Croy, S Bergqvist, T Huxford, G Ghosh, Komives E. Biophysical characterization of the free IκBα ankyrin repeat domain in solution. *Protein Science*. 2004: 1767-1777.

23. SME Truhlar, JW Torpey, Komives EA. Regions of IκBα that are critical for its inhibition of NF-κB· DNA interaction fold upon binding to NF-κB. *Proc Natl Acad Sci USA*. 2006; 103:18951–18956.

24. DU Ferreiro, CF Cervantes, SME Truhlar, Samuel S. Cho, Peter G. Wolynes, Elizabeth A. Komives. Stabilizing IκBα by "Consensus" Design. *Journal of molecular Biology*. 2007; 365:1201–1216.

25. D Krappmann, C Scheidereit. Regulation of NF-κB activity by IκBα and IκBβ stability. *Immunobiology*. 1997; 198:3-13.

26. MP Pando, IM Verma. Signal-dependent and-independent degradation of free and NF-κB-bound IκBα. *Journal of Biological Chemistry*. 2000; 275:21278-21286.

27. EM Schwartz, D Van Antwerp, IM Verma. Constitutive phosphorylation of IkappaBalpha by casein kinase II occurs preferentially at serine 293: requirement for degradation of free IkappaBalpha. *Mol Cell Biol.* 16:3554-3559.

28. JT Kato, M Delhase, A Hoffmann, M Karin. CK2 is a C-terminal IkappaB kinase responsible for NF-kappaB activation during the UV response. *Mol. Cell*. 12:829-839.

29. D Krappmann, FG Wulczyn, CS Huang, A Hoffmann. IkappaBepsilon provides negative feedback to control NF-kappaB oscillation, signaling dynamics, and inflammatory gene expression. *J. Cell Biol*. 173:659-664.

30. B Alvarez-Castelao, JG Castano. Mechanism of direct degradation of IkappaBalpha by 20S proteasome. *FEBS Lett.* 579:4797-4802.

31. K Tenjinbaru, T Furuno, N Hirashima, M Nakanishi. Nuclear translocation of green fluorescent protein-nuclear factor κB with a distinct lag time in living cells. *FEBS letters*. 1999; 444:1-4.

32. Schmid, J. A., Birbach, A., Hofer-Warbinek, R., Pengg, M., Burner, U., Furtmuller, P. G., Binder, B. R. and de Martin, R. Dynamics of NF-kB and IkBa studied with green fluorescent protein (GFP) fusion proteins–investigation of GFP-p65 binding to DNA by fluorescence resonance energy transfer. *J. Biol. Chem.* 2000; 275:17035-17042.

33. Carlotti, F., Chapman, R., Dower, S. K. and Quarnstrom, E. E. Activation of nuclear factor kB in single living mammalian cells. *J. Biol. Chem.* 1999; 274:37941–37949.

34. Carlotti, F., Dower, S. K. and Quarnstrom, E. E. Dynamic shuttling of nuclear factor kB between the nucleus and cytoplasm as a consequence of inhibitor dissociation. *J. Biol. Chem.* 2000; 275, 41028-41034.

35. Asako Sakaue-Sawano, Hiroshi Kurokawa,Toshifumi Morimura, Aki Hanyu, Hiroshi Hama, Hatsuki Osawa, Saori Kashiwagi, Kiyoko Fukami, Takaki Miyata, Hiroyuki Miyoshi, Takeshi Imamura, Masaharu Ogawa, Hisao Masai, and Atsushi Miyawaki. *Cell*. 2008; 132:487–498.

36. Rodriguez MS, Michalopoulos I, Arenzana-Seisdedos F, Hay RT. Inducible degradation of I kappa B alpha in vitro and in vivo requires the acidic C-terminal domain of theprotein. *Mol. Cell. Biol.* 1995; 15(5):2413-9.

37. Palombella VJ, Rando OJ, Goldberg AL, Maniatis T. The ubiquitin-proteasome pathway is required for processing the NF-kappa B1 precursor protein and the activation of NF-kappa B. *Cell.* 1994; 78(5):773-85.

38. Van Antwerp DJ, Verma IM. Signal-induced degradation of I(kappa)B(alpha): association with NF-kappaB and the PEST sequence in I(kappa)B(alpha) are not required. *Mol Cell Biol*. 1996; 16(11):6037-45.

39. Alkalay, I., A. Yaron, A. Hatzubai, A. Orian, A. Ciechanover, and Y. Ben-Neriah. 1995. Stimulation-dependent I kappa B alpha phosphorylation marks the NF-kappa B inhibitor for degradation via the ubiquitin-proteasome pathway. *Proc. Natl. Acad. Sci. USA* 92:10599-10603.

40. Chen, Z., J. Hagler, V. J. Palombella, F. Melandri, D. Scherer, D. Ballard, and T. Maniatis. Signal-induced site-specific phosphorylation targets I kappa B alpha to the ubiquitin-proteasome pathway. *Genes Dev*. 1995; 9:1586–1597.

41. Brockman, J. A., D. C. Scherer, T. A. McKinsey, S. M. Hall, X. Qi, W. Y. Lee, and D. W. Ballard. Coupling of a signal response domain in IkBa to multiple pathways for NF-kB activation. *Mol. Cell. Biol.* 1995; 15:2809–2818.

42. Brown, K., S. Gerstberger, L. Carlson, G. Franzoso, and U. Siebenlist. Control of I kappa B-alpha proteolysis by site-specific, signal-induced phosphorylation. *Science*. 1995; 267:1485-1488.

43. Traenckner, E. B., H. L. Pahl, T. Henkel, K. N. Schmidt, S. Wilk, and P. A. Baeuerle. 1995. Phosphorylation of human I kappa B-alpha on serines 32 and 36 controls I kappa B-alpha proteolysis and NF-kappa B activation in response to diverse stimuli. *EMBO J.* 14:2876-2883.

44. Baldi, L., K. Brown, G. Franzoso, and U. Siebenlist. Mutation of lysines 21/22 in IkB-a block NF-kB activation. *J. Biol. Chem.* 1996; 271:376–379.

45. Scherer, D. C., J. A. Brockman, Z. Chen, T. Maniatis, and D. W. Ballard. Signal-induced degradation of I kappa B alpha requires site-specific ubiquitination. *Proc. Natl. Acad. Sci. USA.* 1995; 92:11259–11263.

46. Alkalay, I., A. Yaron, A. Hatzubai, S. Jung, A. Avraham, O. Gerlitz, I. Pashut-Lavon, and Y. Ben-Neriah. In vivo stimulation of IkB phosphorylation is not sufficient to activate NF-kB. *Mol. Cell. Biol.* 1995; 15:1294-1301.

47. DiDonato, J. A., F. Mercurio, and M. Karin. Phosphorylation of IkBa precedes but is not sufficient for its dissociation from NF-kB. *Mol. Cell. Biol.* 1995; 15:1302-1311.

48. Miyamoto, S., M. Maki, M. J. Schmitt, M. Hatanaka, and I. M. Verma. Tumor necrosis factor alpha-induced phosphorylation of I kappa B alpha is a signal for its degradation but not dissociation from NF-kappa B. *Proc. Natl. Acad. Sci. USA.* 1994; 91:12740–12744.

49. Fenteany G1, Standaert RF, Lane WS, Choi S, Corey EJ, Schreiber SL. Inhibition of proteasome activities and subunit-specific amino-terminal threonine modification by lactacystin. *Science*. 1995; 268(5211):726-31.

50. Fenteany G, Schreiber SL. Lactacystin, proteasome function, and cell fate. *J. Biol. Chem*. 1998; 273(15):8545-8.

51. Sun SC, Ganchi PA, Ballard DW, Greene WC. NF-kappa B controls expression of inhibitor I kappa B alpha: evidence for an inducible autoregulatory pathway. *Science*. 1993; 259(5103):1912-5.

52. Li, X., Y. Fang, X. Zhao, X. Jiang, T. Duong, and S.R. Kain. Characterization of NFkappaB activation by detection of green fluorescent protein-tagged IkappaB degradation in living cells. *J. Biol. Chem.* 1999; 274:21244-21250

53. J Yang, R Yan, A Roy, D Xu, J Poisson, Y Zhang. The I-TASSER Suite: Protein structure and function prediction. *Nature Methods*. 2015; 12:7-8.

54. J Yang, Y Zhang. I-TASSER server: new development for protein structure and function predictions. *Nucleic Acids Research*. 2015; 43:W174-W181.

55. A Roy, A Kucukural, Y Zhang. I-TASSER: a unified platform for automated protein structure and function prediction. *Nature Protocols*. 2010; 5:725-738.

56. Y Zhang. I-TASSER server for protein 3D structure prediction. *BMC Bioinformatics*. 2008; 9:40.

57. Eisenberg D, Luthy R, Bowie JU: VERIFY3D: Assessment of protein models with three-dimensional profiles. *Method. Enzymol*. 1997; 277:396-404.

58. Berman HM, Westbrook J, Feng Z, Gilliland G, Bhat TN, Weissig H, Shindyalov IN, Bourne PE. The Protein Data Bank. *Nucleic acids research*. 2000; 28:235-242.

59. Wu S., Zhang Y. LOMETS: a local meta-threading-server for protein structure prediction. *Nucleic Acids Res*. 2007; 35:3375-3382.

60. Zhang Y., Skolnick J. SPICKER: a clustering approach to identify near-native protein folds. *J. Comput. Chem.* 2004; 25:865-871.

61. Jacobson, M. P., Pincus, D. L., Rapp, C. S., Day, T. J. F., Honig, B., Shaw, D. E., Friesner, R. A. A Hierarchical Approach to All-Atom Protein Loop Prediction. *Proteins: Structure, Function and Bioinformatics*. 2004; 55:351-367.

62. Jacobson, M. P., Friesner, R.A., Xiang, Z., Honig, B. On the Role of Crystal Packing Forces in Determining Protein Sidechain Conformations. *J. Mol. Biol.*, 2002; 320:597-608.

63. Shivakumar, D., Williams, J., Wu, Y., Damm, W., Shelley, J., Sherman, W. Prediction of Absolute Solvation Free Energies using Molecular Dynamics Free Energy Perturbation and the OPLS Force Field. *J. Chem. Theory Comput.* 2010; 6:1509–1519.

64. Guo, Z., Mohanty U., Noehre J., Sawyer T. K., Sherman W., Krilov G. Probing the α-Helical Structural Stability of Stapled p53 Peptides: Molecular Dynamics Simulations and Analysis. *Chem. Biol. Drug Des.* 2010; 75:348-359.

65. Kevin J. Bowers, Edmond Chow, Huafeng Xu, Ron O. Dror, Michael P. Eastwood, Brent A. Gregersen, John L. Klepeis, Istvan Kolossvary, Mark A. Moraes, Federico D. Sacerdoti, John K. Salmon, Yibing Shan, and David E. Shaw. Scalable Algorithms for Molecular Dynamics Simulations on Commodity Clusters. *Proceedings of the ACM/IEEE Conference on Supercomputing (SC06), Tampa, Florida*. 2006; 11:11-17.

66. Harder E., Damm W., Maple J., Wu C., Reboul M., Xiang J.Y., Wang L., Lupyan D., Dahlgren M.K., Knight J.L., Kaus J.W., Cerutti D.S., Krilov G., Jorgensen W.L., Abel R., Friesner R.A. OPLS3: A Force Field Providing Broad Coverage of Drug-like Small Molecules and Proteins. *J. Chem. Theory Comput.* 2016; 12(1):281–296.

67. Jorgensen W.L., Chandrasekhar J., Madura J.D., Impey R.W., Klein M.L. Comparison of simple potential functions for simulating liquid water. *J. Chem. Phys*. 1983; 79:926–935.

68. Michał Rostkowski, Mats HM Olsson, Chresten R Søndergaard and Jan H Jensen Graphical analysis of pH-dependent properties of proteins predicted using PROPKA. *BMC Structural Biology*. 2011; 11:6

69. Björn Wallner and Arne Elofsson. Can correct protein models be identified? *Protein Sci*. 2003; 12(5):1073-1086.

70. Maiti M, Van Domselaar GH, Zhang H, Wishart DS. Superpose: a simple server for sophisticated structural superposition. *Nucleic Acids Res*. 2004; 1(32):W590W594.

71. Chuang G-Y., Kozakov D., Brenke R., Comeau S.R., Vajda S. DARS (Decoys As the Reference State) Potentials for Protein-Protein Docking. *Biophys. J*. 2008; 95:4217-4227.

72. Kozakov D., Brenke R., Comeau S.R., Vajda S. PIPER: An FFT-based protein docking program with pairwise potentials. *Proteins*. 2006; 65:392-406.

73. Y. Zhang, J. Skolnick, TM-align: A protein structure alignment algorithm based on TM-score. *Nucleic Acids Research*. 2005; 33: 2302-2309.